



Resolving anthropogenic aerosol pollution types – deconvolution and exploratory classification of pollution events

Mikko Äijälä¹, Liine Heikkinen¹, Roman Fröhlich², Francesco Canonaco², André S. H. Prévôt², Heikki Junninen¹, Tuukka Petäjä¹, Markku Kulmala¹, Douglas Worsnop^{1,3}, and Mikael Ehn¹

¹Department of Physics, University of Helsinki, Helsinki, Finland

²Laboratory of Atmospheric Chemistry, Paul Scherrer Institute, Villigen, Switzerland

³Aerodyne Research Inc., Billerica, MA, USA

Correspondence to: Mikael Ehn (mikael.ehn@helsinki.fi)

Received: 15 July 2016 – Discussion started: 1 September 2016

Revised: 30 November 2016 – Accepted: 9 January 2017 – Published: 1 March 2017

Abstract. Mass spectrometric measurements commonly yield data on hundreds of variables over thousands of points in time. Refining and synthesizing this raw data into chemical information necessitates the use of advanced, statistics-based data analytical techniques. In the field of analytical aerosol chemistry, statistical, dimensionality reductive methods have become widespread in the last decade, yet comparable advanced chemometric techniques for data classification and identification remain marginal. Here we present an example of combining data dimensionality reduction (factorization) with exploratory classification (clustering), and show that the results cannot only reproduce and corroborate earlier findings, but also complement and broaden our current perspectives on aerosol chemical classification. We find that applying positive matrix factorization to extract spectral characteristics of the organic component of air pollution plumes, together with an unsupervised clustering algorithm, *k*-means ++, for classification, reproduces classical organic aerosol speciation schemes. Applying appropriately chosen metrics for spectral dissimilarity along with optimized data weighting, the source-specific pollution characteristics can be statistically resolved even for spectrally very similar aerosol types, such as different combustion-related anthropogenic aerosol species and atmospheric aerosols with similar degree of oxidation. In addition to the typical oxidation level and source-driven aerosol classification, we were also able to classify and characterize outlier groups that would likely be disregarded in a more conventional analysis. Evaluating solution quality for the classification also provides means to assess the performance of mass spectral simi-

larity metrics and optimize weighting for mass spectral variables. This facilitates algorithm-based evaluation of aerosol spectra, which may prove invaluable for future development of automatic methods for spectra identification and classification. Robust, statistics-based results and data visualizations also provide important clues to a human analyst on the existence and chemical interpretation of data structures. Applying these methods to a test set of data, aerosol mass spectrometric data of organic aerosol from a boreal forest site, yielded five to seven different recurring pollution types from various sources, including traffic, cooking, biomass burning and nearby sawmills. Additionally, three distinct, minor pollution types were discovered and identified as amine-dominated aerosols.

1 Introduction

The field of chemometrics, i.e. “using mathematical and statistical methods [...] to provide maximum chemical information by analysing chemical data” (Kowalski, 1981; Vandeginste, 1982) serves as an important mediator between complex, multivariate chemical measurements and their interpretation. Since the 1970s a variety of chemometric applications have emerged in various fields of mass spectrometry and are common, e.g. in biological and medical implementations, food science and chemical engineering (e.g. Belu et al., 2003; Karoui et al., 2010; Kell, 2004; Pierce et al., 2012; Sauer and Kliem, 2010; van der Greef et al., 2004; Wishart, 2007). Furthermore, aerosol mass spectrometry, al-

though a latecomer among mass spectrometric applications, seems to have been quick in adopting and improving on some of the basic chemometric tools found useful elsewhere, as exemplified by the surge in use of factor analytical techniques for data dimensionality reduction in the recent decade (Canonaco et al., 2013; Lanz et al., 2007b; Zhang et al., 2005, 2011).

Yet, there is a considerable amount of work still to be done in the field of aerosol data chemometric analysis – a significant part of more advanced AMS data analysis is still done manually and thus inevitably limited by the expertise and capacity of the human analyst. In particular, the classification and interpretation of the AMS spectra are still largely based on a dozen or so mass spectral variables called “marker signals” and their ratios (Aiken et al., 2007, 2008; Cubison et al., 2011; Farmer et al., 2010; Mohr et al., 2012). Exploring the logical follow-up to the automatic data dimensionality reduction by applying similar mathematical, computer-aided tools also for un-/semi-supervised classification and identification of AMS spectra, has not been performed outside of the specific application of single-particle mass spectrometric studies (e.g. Freutel et al., 2013; Liu et al., 2013; Murphy et al., 2003; Rebotier and Prather, 2007). Automatic or machine-learning-based classification tools would likely prove invaluable for consistent and objective analysis of a much wider range of AMS data, lessening the outcomes’ dependence on the subjective views of analysts or reliant on their years of expertise in mass spectral interpretation (Ausloos et al., 1999; Ulbrich et al., 2009). Even for an experienced analyst, exploratory data analysis has the potential to uncover previously unknown underlying mathematical structures within the data (Tukey, 1977), offering invaluable clues for the correct selection of solutions and their interpretations.

Sometimes individual, classical analysis methods are used at the edge of their appropriate domain. For example, factor analysis assumes constant profiles over long time frames, when chemical processes actually modify the profiles (Zhang et al., 2011), and hard classification methods can be used for data reduction when observations are non-discrete and form a continuum (Marcolli et al., 2006). More robust results may be obtained by sticking more closely to the core applicability area of each method, where their core assumptions are better expected to hold, and by combining multiple separate methods instead.

More diverse, combined techniques can also overcome inherent limitations of data models. They may, for example, enable the uncovering of the minor, “outlier” aerosol types that often go unnoticed in a long-term factor analysis because of their low relative contribution to total aerosol mass (Ulbrich et al., 2009). Such additional, quantitative information on aerosol chemotypes is widely beneficial for many types of studies involving, e.g. receptor modelling with chemical mass balance or constrained factor analysis models (Belis et al., 2013; Canonaco et al., 2013).

In this work we explore the possibility of complementing the current techniques for AMS data reduction with some analytical and processing methods found to be useful in similar mass spectrometric applications. We apply data dimensionality reduction to deconvolve ambient air pollution events, extracting the characteristic pollution spectra, and subsequently use and optimize unsupervised classification to resolve the pollution types. Our motivations are to (1) test whether a simple unsupervised data clustering method can be used to classify discrete aerosol mass spectral samples without a priori information provided by a human analyst, (2) explore the effect of similarity metric selection and data weighting to optimize data preprocessing (Horai et al., 2010; Kim et al., 2012; Stein and Scott, 1994) and thus enhance the structures in data, leading to improved classification (Anderberg, 1973; Spath, 1980). Finally we will (3) compare which classification measures best capture the differences between different atmospheric aerosol chemotypes, often referred to by the AMS scientific community, and examine how the observed structures in data translate to information on pollution types.

The results on the performance of distance metrics along with the relative importance of variables (optimized weight) for correctly grouping mass spectra can also lead the way towards an automated classification of AMS results against relevant library spectra, as well as providing ways to evaluate and classify (discrete or deconvolved) spectral results in large numbers, such as those often seen in sensitivity analysis or bootstrapping analyses in factor analytical model verification. Indirectly, the information may also help in any manual classification and identification tasks.

We will exemplify the functionality (and hopefully usefulness) of such a machine-learning approach in an analysis of an extensive set of AMS ambient air pollution spectra. We propose that, in this case, the methodology offers an improved way to derive not only reliable, reference spectra for the local, archetypal anthropogenic pollution types, but also quantitative estimates for their expected natural variation. This information has an immediate and direct use, e.g. in constrained factor analytical models that require an input for reference spectra variability (Canonaco et al., 2013).

From an aerosol chemical viewpoint, solid, quantitative knowledge on local pollution types and their chemical characteristics can help decipher and understand a variety of physicochemical observations during times when a site experiences pollution events. Concentrating on individual pollution events also enables the observation and identification of often overlooked minor or rare emission sources, which can provide new information on local or regional atmospheric aerosols.

2 Methods

Although the focus of this study is on statistical analysis of aerosol mass spectrometric measurements, any such venture

is inherently affected by the nature and quality of the experimental data, as well as its preprocessing. We will first provide a short overview of the main features, advantages and shortcomings of the aerosol mass spectrometer instrument (Sect. 2.1) and describe the specific set of data we used (Sect. 2.2) in the testing of the methodology to serve as a background and put into context the choices made when selecting our specific statistical methods and algorithms.

The statistical methods themselves are described in a brief manner in Sect. 2.3, since their in-depth review or commentary is beyond the scope of this article. We encourage the interested reader to follow the references provided for a more comprehensive account and additional background information on the specifics and inner workings of these data analytical techniques and algorithms.

2.1 The AMS instrument and data preprocessing

2.1.1 Compact time-of-flight mass spectrometer (C-ToF-AMS)

The data analysed in this study are acquired with an aerosol mass spectrometer featuring a compact time-of-flight (C-ToF) mass analyser. The instrument is developed and manufactured by Aerodyne Research Inc. (Billerica, MA, US). While outclassed mass resolution-wise by subsequent high-resolution (HR) ToF-AMS variants (Canagaratna et al., 2007; DeCarlo et al., 2006), the C-ToF-AMS mass analyser comes with the highest sensitivity, and thus signal-to-noise ratio (SNR) of any AMS instrument (DeCarlo et al., 2006; Drewnick et al., 2009). This high precision clearly benefits any statistical analysis and partly offsets the smaller number of variables available in unit mass resolution (UMR) data compared to high resolution.

The C-ToF-AMS, described in a thorough fashion by Drewnick et al. (2005), shares many common characteristics with most ToF-AMS instruments – an aerodynamic lens to concentrate the sample aerosol into a tight beam of particles upon entering through the inlet of the instruments, a beam chopper to enable particle size measurement based on their flight time through a vacuum chamber, a thermal vapourizer set at 600 °C to flash vapourize the sample, 70 eV electron impact ionization of the vaporized sample implemented with a tungsten filament, and finally an orthogonal extraction time-of-flight mass analyser to provide the ions' mass spectra.

In the particular C-ToF-AMS we used, the particle time-of-flight (PToF) chamber is considerably shortened (10 cm versus the normal 40 cm chamber). The advantage of this modification is an increased sample transmission from the inlet up to the vapourization and ionization region, at the cost of an increased signal from aerosols' carrier gas, due to the reduction in time and distance for air molecules to diverge from the beam. To combat the effect of an increased number of air molecules passing through the system, a helium flow

is introduced to the PToF chamber to increase the pressure and thus the diffusion of air molecules in the beam passing through the chamber. With this arrangement the air signal is reduced by a factor of 10 to 100, depending on the setting, while only affecting the aerosol signal to a much lesser extent. The helium ions are later removed by an additional high pass mass filter located before the analyser. While not affecting this work, an additional negative effect of this geometry is the reduced resolution in particle time-of-flight sizing caused by the shortened PToF flight track.

2.1.2 Preprocessing of AMS data and derivation of final data matrices

The AMS data need a number of steps and corrections to first compute the per ion mass loading from the raw mass analyser signal, and then to estimate and propagate the errors arising from several sources along the way to the final results. As the general methodology of AMS standard data processing has fortunately been amply described (Allan et al., 2003; Jimenez et al., 2003), as has the derivation of mass spectral matrices and their error estimates (Ulbrich et al., 2009; Zhang et al., 2005), we will only summarize the procedure here and concentrate on the particulars that deviate from the standard approach in our preprocessing.

The AMS data were automatically corrected for changes in m/z axis calibration, using a time-dependent calibration function and a set of around a dozen known marker peaks to fit the time-of-flight to m/z calibration individually to each measured spectrum. The peak areas of all unit m/z signals were then integrated, with manually checked and modified integration regions to yield the background-subtracted signal at each m/z ratio.

The instrument signal response degrade over time was accounted for by using a time period after instrument calibration as a reference point and normalizing the measured air induced signal (airbeam, AB) to the mean value of the reference time (AB_{ref}). The normalization ratio AB/AB_{ref} , describing the instrument response to a known mass concentration of air molecules, was used as a scaling factor for all the measured signals, as suggested by Allan et al. (2003). Due to concerns of non-linearity of the detector response with very high signals typical of N_2 and O_2 , raised by the off-target molecular ratios for air $O_2/N_2/Ar$, argon signal observed at 40 Th was used as a metric for the airbeam intensity.

Airbeam non-linearity in the C-ToF-AMS is discussed in more detail by Hings et al. (2007), who attribute it to signal thresholding affecting low (< 1 ion per MS extraction) signals differently from air ions with multiple ions detected in each extraction.

The AMS fragmentation table was slightly modified to accommodate for the issues arising from the modified PToF chamber and the increased airbeam. Namely some air-related signal ratios used in the fragmentation calculations, such as relative air contribution to observed signals at 15, 29 and

30 Th, were recalculated based on exact molecular ratios obtained from filter runs, automatically performed every 3 h. After this recalibration all the minor, artificial, non-air signals originally seen during filter runs (e.g. in organics and nitrates) at the aforementioned m/z ratios were effectively assigned to the airbeam, excluding them from further analysis.

Efficiency of the ionization process was determined via ammonium nitrate response factor calibration outlined by Jimenez (2003) and Allan et al. (2003). Finally, collection efficiency (CE; Huffman et al., 2005) was evaluated in relation to mass derived from a (twin) differential mobility particle sizer (DMPS; Aalto et al., 2001) after the subtraction of black carbon (BC) given by an aerosol aethalometer (Hansen et al., 1984). The CE correction proposed by Middlebrook et al. (2012) was only applied to one (March 2009) out of the three data sets used in this analysis (see Sect. 2.2), with a small modification to the base CE suggested by the DMPS comparison, as applying it was actually found to slightly weaken the correlation between DMPS and AMS data instead of improving it. For the other two data sets (May 2008, September 2008) a constant CE was applied based on a linear least squares fit to best match the mass observed by the AMS against that derived from the DMPS.

Finally matrices consisting of organic mass spectra and their estimated errors at all measurement points, averaged in data acquisition phase to 5 min intervals, were extracted from the preanalysis software. The error of the organic signals at each time and for each m/z ratio were estimated and propagated to the output matrices using the standard AMS error calculation procedure (Allan et al., 2003; Jimenez et al., 2003) within the AMS Sequential Igor data Retrieval (SQUIRREL; v.1.50) analysis software programmed in Igor Pro (Wavemetrics Inc, Lake Oswego, OR, USA).

The two matrices, one for organic mass spectra and one for the error estimate were additionally preprocessed using the PMF Evaluation Tool (PET; Ulbrich et al., 2009). The preprocessing features mainly take into account an additional correction to the error matrix from electric noise of the instrument, and allow the down-weighting of certain signals with poor SNR or those derived directly from m/z 44 (thus the variation in m/z 44 carrying too much weight in subsequent data analysis by default). The final mass spectral matrices were then used as an input data for the feature extraction algorithm, explained in Sect. 2.3.1.

2.2 Site, measurement campaigns and identification of air pollution events

The experimental data used in this statistical analysis exercise originate from long-term ambient air observations at the SMEAR II station in Hyytiälä, Juupajoki, Finland. The particulars of the measurement campaigns, environment and pollution events are described below.

Table 1. Time frames of measurements and numbers of successfully extracted pollution spectra per data set.

Campaign	Start date	End date	No. of days	Spectra extracted
May 2008	29 Apr 2008	8 Jun 2008	40	23
Sep 2008	10 Sep 2008	15 Oct 2008	35	25
Mar 2009	4 Mar 2009	29 Mar 2009	25	33

2.2.1 SMEAR II field site in Hyytiälä and the EUCAARI measurements

As the practical example of the study is about applying our exploratory data analytical techniques to resolve the archetypal air pollution classes typical of a non-urban field site, we obviously strive for a high-quality, variable and comprehensive set of data to refine and test the methodology. Our data sets of choice originate from the comprehensively documented and characterized station of SMEAR II in Hyytiälä, during the well-covered intensive measurement EUCAARI campaigns of 2008 to 2009 (Kulmala et al., 2009). This already rather familiar data will offer a good test bed for the proposed methodology. Below, both the station and the intensive measurement campaigns are described.

Situated in southern Finland (61°50′40″ N 24°17′13″ E) amidst subarctic pine forest, the Hyytiälä forestry station and the collocated Station for Measuring Ecosystem–Atmosphere Relations (SMEAR II; Hari and Kulmala, 2005) offer an environment that is well representative of the vast taiga biome of northern Eurasia. While not exactly pristine, the surrounding lands are rather unbroken homogenous production forests consisting mainly of typical Scandinavian and Russian taiga tree species: pines (*Pinus sylvestris*) spruce (*Picea abies*), and to a lesser extent birch (*Betula pendula*, *Betula pubescens*) and other deciduous broadleaf species (e.g. species from *Populus*, *Alnus* and *Sorbus* genera). From land use statistics, Williams et al. (2011) estimate that 94 % of the local (5 km radius) and 90 % in the nearest 50 km land area consist of forested land (including forest at seedling or sapling state). The nearest town of Orivesi (pop. 9500) lies 19 km due south of the station and the city of Tampere (pop. 213 000), ca. 48 km to the south-west. The surrounding county of Juupajoki is sparsely populated (5–10 inhabitants per km²) and while it does have some local sources of anthropogenic air pollution, such as household heating and cooking, they are generally very limited in terms of magnitude and geographical breadth.

A notable exception to the absence of major anthropogenic pollution sources in the local environment are the two lumber mills and the wood pellet factory in the small village of Korkeakoski, 7 km east-south-east from Hyytiälä, and the other small sawmills further away, which do have a marked influence on the volatile organic compounds (VOC) concentra-

tions and aerosol population of Hyytiälä when the incoming air mass is advected over these mills (Eerdekens et al., 2009; Liao et al., 2011). Additionally, although the local aerosol sources such as passing vehicles, cooking emissions at the forestry station, nearby cottage, household or sauna heating are negligible on a large scale, they can momentarily affect the local air quality if emitted from close enough not to be diluted below the detection limits, and are thus detected by many of the more sensitive, high-time-resolution instruments at the SMEAR II stations.

Nevertheless, the preeminent cause of degraded air quality (relative to the background) at the station is the medium-to-long-range air convection from industrialized areas of southern Finland, the St. Petersburg region in Russia in particular (Kulmala et al., 2000; Patokoski et al., 2015; Riuttanen et al., 2013) and even all the way from the industrial heartlands of (mostly eastern) continental Europe (Niemi et al., 2009; Sogacheva et al., 2005).

As it is independent of these anthropogenic components, the local atmosphere is always influenced by the ever-present biogenic background aerosol and biogenic volatile organic compounds (BVOC). These exhibit their own seasonal and diurnal variations. BVOC concentrations are generally high, both during the afternoon due to maximum emissions and at night-time due to the trapping of emissions in the shallow, unmixed boundary layer (Rinne et al., 2005). The aerosol biogenic particle mass was also higher at night due to thermally driven condensation of semi-volatile species into existing seed particles. Due to the biological origin of the natural aerosol, the biogenic aerosol background is obviously higher in warmer months (e.g. Patokoski et al., 2014).

The relative lack of local anthropogenic sources and their pronounced dependence on air mass origins, manifesting as observations of isolated aerosol and gas phase plumes, make Hyytiälä an ideal natural laboratory for studying the effects and characteristics of local and transported air pollution on the otherwise clean atmosphere over the expansive subarctic biomes.

The EUCAARI study, conducted from 2007 to 2010, aimed at examining the interactions between air pollution and climate change (Kulmala et al., 2009). The results have been widely published (see Kulmala et al., 2011, for a summary of findings) and include discussions, e.g. on aerosol source apportionment and chemical ageing (Kulmala et al., 2011; Ng et al., 2010b). The intensive observation periods of the project took place in spring 2008, autumn 2008 and late winter 2009. The exact time frames of the AMS measurements are available in Sect. 3.1, Table 1.

An especially comprehensive analysis of the intensive EUCAARI AMS data is written by Crippa et al. (2014), providing a reference point to compare our results with. Their analysis provides plausible estimates of aerosol speciation using consistent methodology. Due to the obvious limitations induced by the very large number of data sets and the somewhat rigid methodology of using general reference spectra

from quite different types of environments for all the sites and by applying rather strict constraints to their allowed variability, it is possible for the analysis to miss out on some divergent, locally relevant phenomena. As an additional motive for this work, we aim to provide considerably enhanced prerequisite information for applying such a factor analytical methodology to an individual site, by observing the local anthropogenic aerosol characteristics and variation, and tailoring the input reference spectra and variation estimates accordingly.

2.2.2 Identification and selection of air pollution events

The term “air pollution event” is in the context of this study defined loosely as a period of significantly increased concentrations relative to a stable background aerosol. This implies that the pollution episode has a distinct beginning, a point in time when a relatively stable background aerosol is first complemented with a specific pollution aerosol, and an end, when the pollution vanishes, leaving a background aerosol similar in composition and mass to that observed before the event. During the pollution episode we assume the observed total aerosol is a two- (or in some cases multi-) component superposition of background and chemically invariable “pollution plume” aerosols. Although there are undoubtedly aerosol dynamical processes going on between the two aerosol types, the background and the plume, we assume these to be of minor importance due to the generally short time frames of the events. Some examples of typical pollution event types and durations are given in the results (Fig. 1).

When basing the pollution event definition on aerosol mass, while we can pick out the clearest instances of pollution with confidence, we run into problems when the increase in mass concentration approaches the magnitude of noise in the instrument. Also, after pollution events that last a better part of a day or longer, it is questionable whether the background aerosol has remained the same and whether it is even possible to describe the changing pollution unambiguously. To address these issues of demarcation, we needed to define further conditions to separate real pollution from short instrument noise peaks on one hand and long periods of increased concentrations of gradually changing or evolving pollution aerosol on the other. Hence, the qualitative requirements of a pollution episode to be accepted for our analysis were set as follows.

1. A distinct temporary rise of organic aerosol mass concentration above background level.
2. The ability to unambiguously separate the pollution plume from the background.
3. The supposed pollution spectra needs to be physically reasonable (i.e. not a minor spike of instrument noise).

The above criteria were taken as qualitative, and their fulfilment evaluated visually from the time series and mass spec-

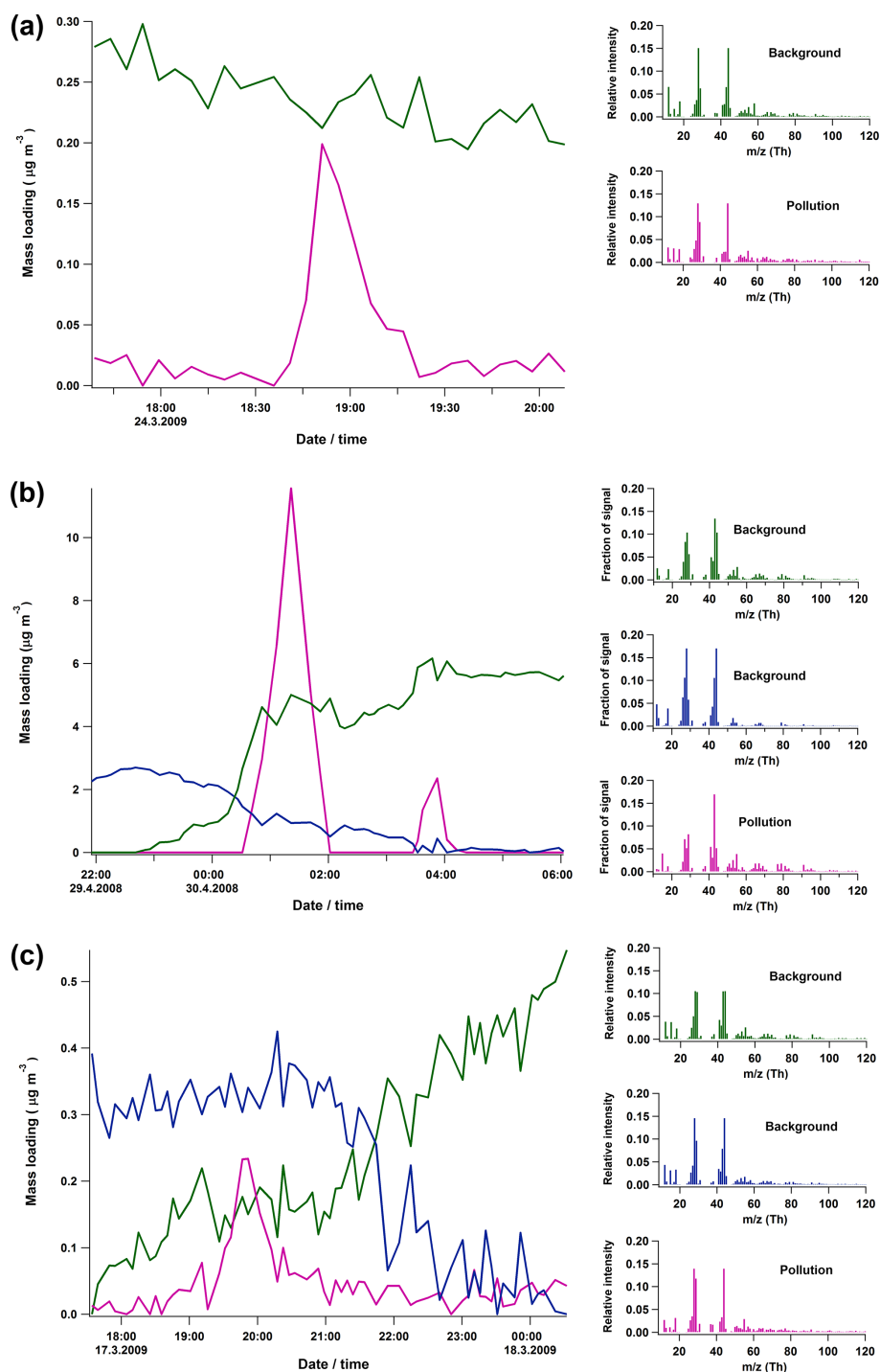


Figure 1.

tra. Still, some rough guideline values for required plume features are given below to convey the magnitudes of the thresholds used in our manual event screening.

A rough estimate of a 10% rise of plume peak mass versus surrounding background aerosol mass was taken as an approximate threshold for criterion 1 selection. The timescales

considered ranges of pollution events from minutes (two data points equalling 10 min) to several days (maximum was 5 days, in the case shown in Fig. 1d). The first criterion can thus be considered lax and likely overly inclusive. Criterion two was much stricter and in practice required the deconvolved pollution time series to exhibit a small enough corre-

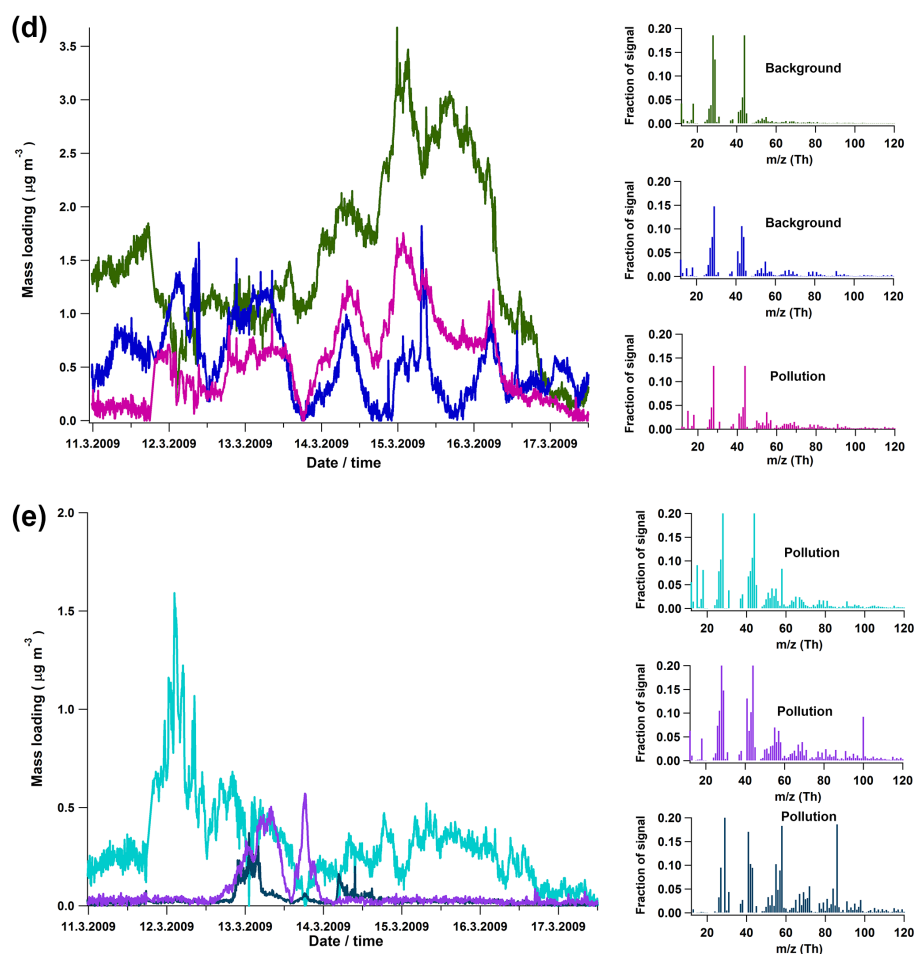


Figure 1. Examples of time series of extracted PMF factors for four different pollution cases, ranging from simple to very complex cases. (a) A simple, clear case with stable background. (b) An example of a well-resolved extraction with a repeating pollution plume and two changing background factors. While the factors are marginally correlated, the separation is still considered clear. (c) An extraction of a weaker pollution plume factor from two temporally changing background factors. The complex event shown in (d, e) is a borderline accepted case due to its long duration (criterion 1; Sect. 2.2.2) and presence of several pollution types (criterion 2), but was eventually accepted to the analysis due to the clear temporal and chemical separation of the pollution factors.

lation between the temporal behaviours of plume and background aerosols: in the background time series a low level of jitter around mean background mass during the plume was accepted in mild cases, as long as it did not contain marked dips (anti-correlation) or hills (correlation) matching or mirroring the plume behaviour. The approximate limit was that the (anti-)correlation should not affect the pollution factor mass by more than $\pm 20\%$ due to the mass misapportionment between plume and background. An example of such minor, but accepted positive correlation is seen in Fig. 1d. Additionally, the pollution was required to vanish (average mass concentration $< 10\%$ of factor peak mass) at the background periods before and after the event. The third criterion meant that, on a practical level, all the spectra were required to not resemble white noise, contain only a single variable signal or conduct similar abnormal behaviour that would probably arise from technical issues or analysis artefacts (i.e. factor

splitting). These stricter criteria (2 and 3) disqualified an estimated one-third of the sample events fulfilling criterion 1.

We note that stricter, fully qualitative and preferably statistics-based limits for event screening would certainly be preferential, and might enable automatic event identification. From a more quantitative analysis the exact uncertainty induced in this sample selection process could be also derived. Our rough estimate for the magnitude of maximum uncertainty is the 20% deriving mainly from the effect of mass misapportionment allowed in the correlation examination phase (criterion 2). Unfortunately, due to the chemometric focus of this study, a more exhaustive time-series-based analysis of the phenomenon of air pollution plumes was not achieved here.

It should be noted that, while the first and third conditions could be examined using a simpler non-statistical analysis method like background subtraction, there are many

pollution episodes where this would not suffice. While we could define the pollution-plus-background spectrum from the event period and the background spectrum as an average of background before and after the event, and subtract the latter from the previous, yielding the characteristic pollution spectrum (e.g. in Fig. 1a) the second condition is much more problematic if the background varies, not even necessarily in a linear way, or several pollution plumes overlap (e.g. shown in Fig. 1d). This especially applies to events with a long duration, from several hours to even a couple of days, and to events with multiple consecutive peaks, which still represent the same event (case in Fig. 1b). To account for these complications we feel a more advanced data reduction method, such as the factor analytical approach presented in Sect. 2.3.1, is indeed required to be able to thoroughly evaluate which of the events satisfy our selection criteria.

2.3 Statistical analysis tools

As numerous studies have already been conducted on feature extraction and data dimensionality reduction in connection with AMS results (Ng et al., 2010a; Zhang et al., 2011), in this work we will focus more on classification and identification techniques suitable for AMS data.

Based on a brief review of suitable data analytical methods, we selected the specific methods and algorithms used in this work: for pollution feature extraction we selected a model already tried and tested for AMS data, the positive matrix factorization (PMF; applying the ME-2 algorithm; Paatero, 1999) and for feature classification we use the elegantly simple and long-established *k*-means clustering algorithm (MacQueen, 1967). While there exist favourable reviews for PMF as a data reducing/receptor model, for AMS studies (e.g. Hopke et al., 2016) no similar reviews were found to suggest a preferential clustering algorithm for AMS data. As *k*-means is often considered a default algorithm for approaching a multitude of classification problems, we selected it for this AMS spectra classification exercise. While it will provide a baseline with which to compare future results, *k*-means may not be the optimal algorithm for this purpose, and a comprehensive evaluation of suitably different algorithms would certainly be beneficial in future spectra classification studies.

In this work we will use PMF in a non-classical way, to extract characteristic air pollution spectra from air pollution plumes, which are often considered to be anomalous data and discarded from long time series analyses. As there often exists considerable variation among mathematically equally good PMF solutions, termed "rotational ambiguity" (see Supplement Sect. S1), the issue of selecting the correct solution needs to be resolved. We propose that in the context of this work, selecting the PMF solution with non-correlating time series of plume and background can be used to identify the rotation that best separates the characteristic pollution factor, and thus largely avoids the factor analytical models'

inherent weakness of rotational ambiguity, which also afflicts PMF (Paatero et al., 2014). We will then demonstrate classification of the extracted spectra to aerosol types using *k*-means clustering, and study the effects of simple data preprocessing options and basic metrics for spectral (dis)similarity on these classification solutions.

2.3.1 Positive matrix factorization (PMF) and its application to studying air pollution plumes

In the analysis of aerosol mass spectrometric results, data reductive methods are put to good use for reasons explained in the introduction. To respond to the challenges and requirements posed by the AMS data, experts in statistics and modelling have updated many traditional analysis tools and developed new ones to answer the specific needs of this type of environmental data analysis. Perhaps the best-known technique developed specifically for feature extraction from environmental, multidimensional data is the use of the positive matrix factorization (PMF) model to deconvolve and interpret the enigmatic organic aerosol chemistry reflected by the often complex AMS mass spectra.

The PMF technique developed by Paatero and Tapper (Paatero, 1997; Paatero and Tapper, 1993, 1994) is an iterative, factor analytical model to explain observations at a receptor site, i.e. time series (*t*) of variables (*v*) (in form of a size $t \times v$ matrix **X**), using a bilinear combination of temporal behaviour of loadings of factors (*f* in a $t \times f$ matrix **G**) and the factors' time-invariant profiles (an $f \times v$ matrix **F**), describing composition. If then **E** denotes the unexplained residual, the difference between the model (**G** × **F**) and the observations (**X**), the PMF model can be formulated

$$\mathbf{X}_{(t \times v)} = \mathbf{G}_{(t \times f)} \times \mathbf{F}_{(f \times v)} + \mathbf{E}_{(t \times v)}, \quad (1)$$

where the subscripts indicate the sizes of matrices corresponding to the number of points in time series (*t*), number of factors (*f*) and number of variables (*v*). While *t* and *v* are decided by the set of data available (and possible preprocessing), *f* is essentially a free parameter selected by the analyst, as is apparent from Eq. (1). Importantly, in PMF all the entries in each of these matrices are limited to positive values, corresponding to environmentally relevant loadings and profiles being non-negative. This considerably reduces the number and variety of mathematical solutions to the modelling problem, and helps to effectively filter out some of the physically unrealistic, negative solutions (Paatero, 1997).

One of the noteworthy improvements, summarized in detail by Paatero and Tapper (1994), over previous feature extraction methods such as principal component analysis (PCA; Hotelling, 1933; Jolliffe, 1986; Pearson, 1901) is that the PMF model does not blindly minimize **E**, but rather the weighted residual. This allows for a better measure of the amount of variation not explained by noise from the experimental measurement, denoted by the standard deviation of variables (a size $t \times v$ matrix σ).

Therefore, for the objective function to be minimized, \mathbf{Q} can be written

$$\mathbf{Q}_{t \times v} = \sum_{i=1}^t \sum_{j=1}^v \left(\frac{\mathbf{E}_{i,j}}{\sigma_{i,j}} \right)^2. \quad (2)$$

That is, the squared residual to be minimized is effectively scaled by the variance of each point in the matrix.

PMF analysis is performed for each air pollution event (defined in Sect. 2.2.2) individually. The time window of the analysis period is selected around the event to include both the pollution episode and some background before and after the event. The advantage of studying this type of relatively short-term phenomena is that we can easily evaluate the fulfilment of the criteria outlined in Sect. 2.2.2, and we can additionally discriminate between mathematically equal solutions, mostly evading the issue of rotational ambiguity. Essentially, knowing beforehand what the (qualitative) temporal behaviour of a pollution and background factors should be like (i.e. the time series of the factors should be uncorrelated), we can explore a number of factors and the solution space to select the solution best fulfilling our criteria of physical correctness. By adhering to these criteria, we strive to minimize the ambiguity related to our selection of solutions, as well as considerably reduce the effect of subjectivity with regard to selecting solutions.

The uncertainties and limitations in PMF are related to measurement errors, uncertainty in data and modelling errors of the PMF bilinear model and rotational ambiguity of the PMF results (Paatero et al., 2014). Rotational uncertainty is inherent to all linear algebraic, factor analytical models (Henry, 1987) and arises from the existence of several model solutions of mathematically equal rates of explanations of the observations. Rotational ambiguity was decreased or even eliminated as the number of zero values available in the data increased (Anderson, 1984; Paatero and Hopke, 2009), making this type of plume modelling by PMF propitious (as the background regions contain ample observations close to zero concentrations of plume chemical constituents). The topic of rotational ambiguity is discussed in more detail, and further references are available in the Supplement (Sect. S1). The modelling errors in PMF relate to simplifications and unrealistic assumptions (e.g. unchanging factor profiles in PMF, translating to neglecting the effect of atmospheric chemistry on mass spectra). Paatero et al. (2014) note that the effect of measurement (random) errors along with rotational uncertainty decrease (in cases where there are more zero values available in larger data) with increasing data set size, while the modelling errors are exacerbated.

Regarding the PMF uncertainties overall, we propose that aerosol plume and pollution event modelling of AMS data by PMF generally decreases analysis uncertainty compared to analysing the full time series, specifically in our case of high SNR data with small random errors. The higher rotational ambiguity induced by having a smaller set of data is offset by the abundance of zero values in concentrations,

while the modelling errors from the neglect of chemistry are decreased due to shorter analysis time windows. Additionally, the selection of solution and rotation is facilitated by the external, physical criterion of minimal correlation of factor time series. We propose that using the [modulus of] correlation minimum as a guideline for rotation selection resolves the physically correct rotation (source-wise differentiation of factors) from among the ones available in the solution space.

An inherent feature of factor analytical receptor models is also that they are unable to separate components with a high degree of correlation in profiles (spectra) or loadings (mass concentration) (Henry et al., 1984). This problem of multicollinearity hinders or even prevents the extraction of spectra from individual sources that are collocated. In such a case a mixed air mass, e.g. one transported from an urban location with multiple sources (traffic, cooking and combustion) would be resolved as a single factor, the characteristic spectra which would be a linear sum of the actual, single sources. A similar effect, profile-wise, occurs with extensive oxidation of organic aerosol components – the spectral similarity of organic aerosol increases upon atmospheric oxidation, leading to difficulties in differentiating between highly oxidized aerosol types, even if they originate from chemically distinct emissions (Ng et al., 2010b; Zhang et al., 2011). Both of these effects are likely to impact negatively on data reduction achieved by PMF and can carry over to clustering, which by default assumes discrete or deconvolved samples.

Nevertheless, we should be warranted in expecting that not all the sources are similarly collocated; thus some extracted samples indeed represent “pure” spectra from single sources (e.g. a passing car or an individual aerosol plume from a single smokestack close by). This would allow identification and proper handling of the mixed plumes within the framework of sample classification and weighting, covered in the next Sect. 2.3.2 and 2.3.4). We will evaluate and address these issues further in light of results in Sect. 3.4 and 3.6.

2.3.2 The k -means algorithm

K-means clustering is one of the most popular, widely used and well-known classification algorithms developed as far back as the 1950s and 1960s (Ball and Hall, 1965; MacQueen, 1967; Steinhaus, 1956). It is a simple iterative partitioning clustering algorithm that partitions a set of objects in a multidimensional space into a preset number (k) of clusters based on a distance (or dissimilarity) metric. For each cluster resulting from any partitioning solution we can calculate a quantity measuring the cluster cohesion, a within-cluster sum of squared distance between the calculated cluster centre μ_n (of a cluster c_n) and all member objects x_i assigned to it. In Euclidean space we get the following:

$$J(C_n) = \sum_{x \in C_n} \|x_i - \mu_n\|^2. \quad (3)$$

The k -means algorithm tries to minimize this quantity $J(C_n)$ summed over all clusters k , which we denote $J(C)$:

$$J(C) = \left(\sum_{n=1}^k J(C_n) \right). \quad (4)$$

The iterative procedure of k -means is briefly described in the Supplement (Sect. S2). Upon convergence with a solution, i.e. global or local minimum of $J(C_n)$, the output of the algorithm gives the user the final assignment of points to clusters, the cluster centroid locations c as well as distances from each data point to all other points and the cluster centres. These distances can be used to evaluate the quality of both the entire clustering solution and the cohesion and variance of individual clusters. It is important to note that k -means converges on any minimum of Eq. (4) found, regardless of whether it is global or local. Finding the global minimum is not guaranteed but can be made more probable by performing repetitive clustering with different initializations for starting cluster centres and selecting the result with lowest $J(C)$.

Further discussion on the selection of user parameters for k -means initialization and cluster numbers is presented in Sect. 3.2 and in the Supplement (Sect. S2). For this analysis we used a k -means algorithm applying an improved initialization method (k -means++; Arthur and Vassilvitskii, 2007), and the number of clusters (k) was kept as a free parameter within a range of $k = 2$ to 20. The selection of dissimilarity metric parameters is discussed below.

2.3.3 How to define (dis)similarity of mass spectra

Among the most important questions in clustering is the selection of a measure for distance or (dis)similarity between two objects, a topic for which there are both theoretical (Anderberg, 1973) and experimental (e.g. Stein and Scott, 1994) considerations to be taken into account. Fortunately for the choice of metric we have plenty of recommendations available for our selection: there are several guidelines and recommendations (e.g. Cormack, 1971; Gordon, 1999; Kaufman and Rousseeuw, 2009) available of which similarity metric best to apply for various types of problems, including problems related to identification, comparison and classification of mass spectra similar to ours. As an experimental basis for the metric comparison we cite the informative and thorough study by Stein and Scott (1994) of NIST Mass Spectrometry Data Center, the conclusions of whose are covered in wider detail further below. Importantly, the distance metric selected needs to be mathematically compatible with the type of variable on hand. This point in question is addressed in Sect. S3.

Some common approaches available for and often used as distance (d) metrics include the following:

1. the squared Euclidian distance

$$d(u, v) = \sum_{i=1}^n \|u - v_n\|^2, \quad (5)$$

2. the city block distance (or “Manhattan distance”; Johnson and Wall, 1969; Carmichael and Sneath, 1969)

$$d(u, v) = \sum_{i=1}^n \|u - v_n\|, \quad (6)$$

3. the cosine distance (Sokal and Sneath, 1963)

$$d(u, v) = 1 - \frac{u \times v}{\|u\| \|v\|}, \quad (7)$$

4. the correlation distance (Fortier and Solomon, 1966; McQuitty, 1966; Sokal, 1958)

$$d(u, v) = 1 - \frac{\sum_{i=1}^n (u_i - \bar{u})(v_i - \bar{v})}{\sqrt{(\sum_{i=1}^n (u_i - \bar{u})^2)} \sqrt{(\sum_{i=1}^n (v_i - \bar{v})^2)}}, \quad (8)$$

where u and v are n -dimensional vectors corresponding to objects (with the subscript n here corresponding to the m/z variables), and \bar{u} and \bar{v} are the mean of variables in u and v . Although often called “distances”, the squared Euclidean, cosine and correlation measures are, strictly speaking, not distance metrics, as they violate the triangle equality required for a proper distance metric, and should be considered instead measures (metrics) of dissimilarity between a pair of objects (Anderberg, 1973; Spath, 1980). Other metrics obviously exist as well, but as a comprehensive review is out of the scope of this work, we limited our comparison to these common metrics available in our analysis software (Matlab 2015a, MathWorks Inc., Natick, MA) standard functionality.

Additionally to experimentally evaluating the metrics, Stein and Scott (1994) recommend data-weighting methods such as signal intensity scaling and mass scaling to be examined. They find modest improvement of a couple of percent accuracy in the dot product (cosine) and Euclidean-based matching when scaling the signal intensities by their square root to emphasize smaller signals, or when scaling all the signals by a power of their “mass” (i.e. m/z ratio), placing more weight on the higher m/z signals as a preprocessing measure. For intensity scaling the weight given to a variable (signal at m/z) can be expressed as

$$\text{weight}_{\text{intensity}} = \sqrt{[s_i]_{\text{signal}}}, \quad (9)$$

where s_i is a (root function) intensity scaling factor. For mass scaling the variable weights are given by

$$\text{weight}_{\text{mass}} = \left(\frac{m}{z} \right)^{s_m}, \quad (10)$$

where $s_m (> 1)$ is a mass scaling factor for the variable locations (m/z). We also test these in connection to our data and report the results in Sect. 3.2.3.

Although the theory and literature seem to favour the cosine (dis)similarity as a measure of mass spectral objects' associations with each other, we ran several comparisons using different parameters for *k*-means++ and present the results in Sect. 3.2. To objectively evaluate and interpret the classification results, we additionally pursued a metric other than an expert opinion for measuring the quality of a solution. Some alternative evaluation options are discussed and our method of choice, the silhouette examination, is presented below.

2.3.4 Silhouettes in evaluation and interpretation of clustering solutions

To evaluate and, to an extent, validate the clustering analysis we need an objective, diagnostic metric to compare different results. There are several alternatives available, four of which we tested in relation to this work. We considered the four evaluation criteria available in the Matlab software statistics toolbox (R2015a), namely the silhouette (Rousseeuw 1987), Calinski–Harabasz (Caliński and Harabasz, 1974), Davies–Bouldin (Davies and Bouldin, 1979) and gap (Tibshirani et al., 2001) criteria, the evaluation results of which are presented in Sect. S4, Figs. S2 to S4.

The downside of the three latter methods is that they do not (at least unmodified) accept all non-distance dissimilarity metrics such as the cosine (dis)similarity. For squared Euclidean distance, which was compatible with the evaluation functions, the methods yield mixed results. Upon examining the *k*-means solutions as described below in the results section, as well as looking at theoretical considerations (Sects. 2.3.3, S3), we feel the use of non-Euclidean metric may indeed be recommendable, and that the silhouette criterion does manage to convincingly identify the number of “natural”, physically reasonable aerosol types (clusters) – therefore we will opt for using the silhouette value criteria detailed by Rousseeuw (1987) in our evaluation of the clustering results of this work.

Rousseeuw (1987) defines for each object *i*, belonging to cluster A and having B as the nearest-neighbouring cluster, a silhouette value of *s*(*i*):

$$s(i) = \begin{cases} 1 - \frac{a(i)}{b(i)}; & \text{for } a(i) < b(i) \\ 0; & \text{for } a(i) = b(i) \\ \frac{b(i)}{a(i)} - 1 & \text{for } a(i) > b(i) \end{cases}, \quad (11)$$

where *a*(*i*) is the average distance to all other objects of the same cluster (A), and *b*(*i*) is the average distance to all objects of the closest neighbouring cluster (B). For a singleton cluster containing only one object, *a*(*i*) is not well defined. Rousseeuw puts *s*(*i*) to zero in this case, but other conventions exist that use a silhouette of one for singletons.

The silhouette value has some convenient properties for interpreting the quality of the clustering assignments that can be applied on single-point, cluster and total solution levels.

When *s*(*i*) is close to unity, the within-cluster dissimilarity *a*(*i*) is much smaller than the between-cluster dissimilarity *b*(*i*), indicating the point is very likely correctly grouped, and conversely, classifying the point the next nearest cluster would be a much poorer choice. On the other hand, if *s*(*i*) is close to -1 , it signifies that the next best clustering choice would actually be a much better one than the current assignment; i.e. the point is on average more similar to the points in the neighbouring cluster than to the points in its assigned cluster. This implies that the point is likely misclassified. If *s*(*i*) is close to zero, the point is situated between clusters, and it is not at all clear to which it belongs – its dissimilarity to both of the groups is about equal ($a(i) \approx b(i)$).

The average *s*(*i*) of points in a cluster of average silhouette width expresses if a cluster is clear cut or weak: the higher the average cluster silhouette width, the more pronounced the cluster. A graphical representation displayed in the Supplement (Fig. S5). The overall silhouette width is the average *s*(*i*) of all the objects and can be used as a parameter to judge the overall quality of the clustering solution. Maximizing the overall silhouette value can be used to evaluate the “natural” number of clusters in the data (Rousseeuw, 1987), an approach we will also utilize in this work. Some further notes on silhouette values can be found in the Supplement (Sect. S5).

2.3.5 Posterior processing – weighting cluster centres and deriving within-cluster variation

The *k*-means algorithm yields a list of assignments of all objects to clusters and defines the cluster centres as the arithmetic mean of the objects within the cluster. These artificially constructed centres can be used to denote the average object within that cluster. However, this approach is subject to one of the main weaknesses of *k*-means: the susceptibility to outliers, borderline cases and outright misclassifications affecting the cluster centre location in the same way as the objects that would be considered very appropriately clustered. These derive directly from the simplistic functionality of the *k*-means algorithm (Sect. 2.3.2), and therefore there is little to be done to alleviate the issues outside of selecting another algorithm.

Nevertheless, we do have additional, diagnostic information available to us outside of the simple list returned by the *k*-means algorithm; in the form of the silhouette value information calculated from the assignment listing combined with the dissimilarity matrix. In this work we aim to utilize the statistical information available to us to the fullest, and in the spirit of this goal we apply a simple post-processing step to derive weighted centroid objects to represent the groups of objects in a more robust, classification error-resistant way.

Assuming the objects nearer the cluster centre are a better representation of the class than the ones on the edges, or indeed the ones likely misclassified, they should carry more weight when a typical representative of the class is

selected or constructed. In this work we construct characteristic centroid objects, i.e. spectra, by taking a weighted arithmetic mean of the cluster members instead of the original, unweighted sample mean. As a weight we use the silhouette values indicating the confidence we have on the representability of the object. Any likely misclassified objects with negative silhouette values have their weight set to zero. The weighted cluster centroid C_w can be expressed as

$$C_w = \frac{\sum_{i=1}^n u_i w_i}{\sum_{i=1}^n w_i}; \quad w_i = \max(0, s(i)), \quad (12)$$

where u_i are the cluster member objects and w_i the respective weights, i.e. the non-negative silhouette values $s(i)$ obtained from Eq. (11). Similarly we obtain a weighted standard deviation σ_w for a measure of the within-cluster variation. With a Bessel correction (Gauss, 1823) for small-sample variance, we can write for the weighted standard deviation:

$$\sigma_w = \sqrt{\frac{\sum_{i=1}^n w_i (u_i - C_w)^2}{\sum_{i=1}^n w_i - \frac{\sum_{i=1}^n w_i^2}{\sum_{i=1}^n w_i}}}. \quad (13)$$

The change in mass spectrum induced by the weighting was determined to be extremely low, as can be seen comparing the unweighted and weighted spectra, exemplified in the Supplement, Fig. S6. For the final spectral solution presented in this work, the similarity (r_s^2 , [Pearson] coefficient of determination for mass-scaled spectra) between the scaled and unscaled centroids was found to range from 0.994 to 1.000, confirming that weighting by silhouette does not markedly alter the resulting spectra.

Overall the variabilities represented by the weighted standard deviations are generally smaller than the unweighted ones, due to the down-weighting of outlier objects' influence. The aim of this post-processing is to derive more representative characteristic mass spectra for the pollution types, and to decrease the error from the ambiguity of the classification. This should allow us to derive plausible estimates for the actual natural variation within a specific aerosol type.

3 Results and discussion

In the following chapter, we present some examples of pollution spectrum extraction (Sect. 3.1), and evaluate the similarity and weighting parameters used for their subsequent grouping (Sect. 3.2). We then offer an aerosol chemical interpretation for the different aerosol types (clusters) for the grouping we consider most realistic (Sect. 3.3 and 3.4) and further try to understand and interpret the metastructure of clustering solutions, i.e. how the solutions relate to each other, what drives them and how they are related to divisions in chemical characteristics (Sect. 3.5). Finally some basic estimates of natural variability within the pollution types are given in Sect. 3.6.

3.1 Extraction of pollution spectra

Although time consuming, applying the pollution feature extraction approach (described in Sect. 2.3.1) to the identified pollution events (Sect. 2.2.2) allowed us to extract the pollution factors' spectral profiles. Applying our simplistic selection criteria to find the most physically correct rotation among the solutions, we hope to have minimized the rotational ambiguity, as well as the need for subjective choices by the analyst. Following the procedure described in Methods, we managed to extract a total of 81 characteristic mass spectra, corresponding to as many unique pollution plumes. In the Supplement, namely the local time and above-canopy wind direction taken at the time of peak mass concentration was recorded for all plumes. The background spectra were not further considered in this analysis. The per-campaign distribution of the successfully extracted pollution events are presented in Table 1.

Some examples of factor time series of various types of accepted extractions are given in Fig. 1, illustrating the considerable (temporal) variability in the types and conditions of pollution events, e.g. from a single plume with a stable background (Fig. 1a) to very complex events with multiple overlapping plumes (Fig. 1d and e).

3.2 Evaluation of clustering parameters and preprocessing options

As discussed in Sect. 2.3.2, there are several options for the standard k -means clustering, particularly in terms of data preprocessing, selecting the number of clusters and the distance metric, but also in specifying the number of repetitions, type of clustering initialization and treatment of empty clusters during the iteration process. In the course of data analysis, we explored the effects of these parameters and preprocessing options on the quality of our clustering solutions and their general structures.

3.2.1 General clustering parameters

We note that using a low number of repetitions (< 10) does not reliably return the exact same optimal solution, so there seem to be several similar, but non-identical, local minima as well as the global one for k -means to convergence on. A hundred or a thousand repetitions already seem to offer consistent and reproducible results. In evaluating the effects of preprocessing, 1000 repetitions were used and in a calculation of the results selected for detailed chemical evaluation (Sect. 3.4), the algorithm was run 10 000 times.

The clustering initialization method was not found to notably affect our results in any way, at least with a generally high number of repetitions. Due to literature recommendations based on comparison (Shindler, 2008), the k -means++ initialization by Arthur and Vassilvitskii (2007) was selected for use.

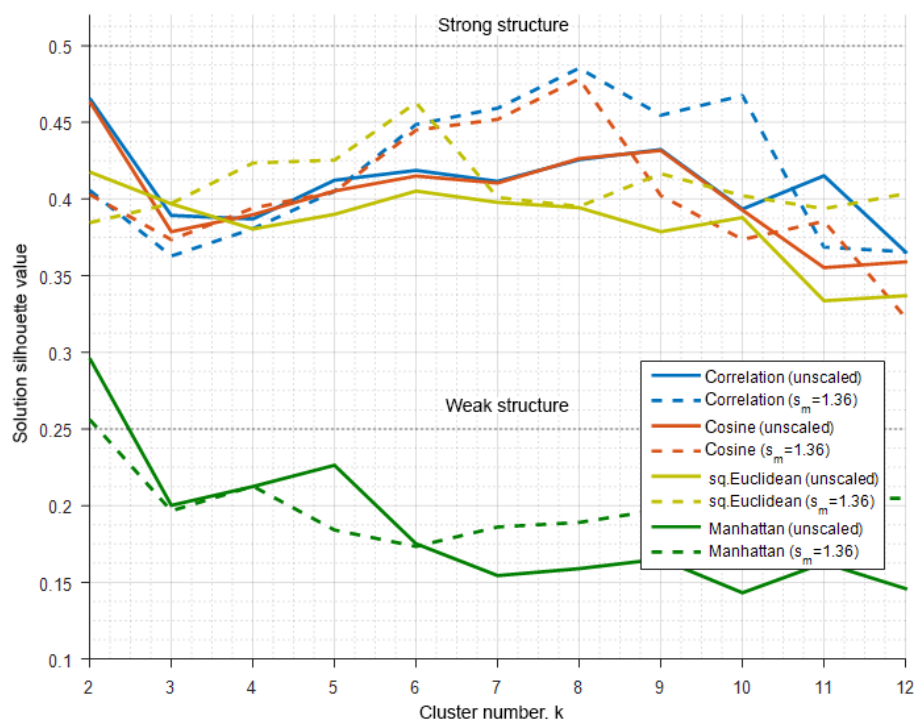


Figure 2. Solution silhouette value of clustering solutions for $k = 2$ to $k = 20$, for the four dissimilarity metrics (colour coded). The solid lines depict solution silhouette values for unscaled data and the dashed lines represent the solution qualities for when data weighting is applied (non-optimized mass scaling, $s_m = 1.36$; Sect. 2.3.3). The 0.25 and 0.50 limit (dotted black lines) indicate lower limits above which we could expect weak (silhouette 0.25) and strong (0.50) structures to exist in the data (Kaufman and Rousseeuw, 2009; Sect. 2.3.4).

We set the additional option “empty cluster action”, i.e. what would happen if an empty cluster is created in the course of the iterative process, as a “singleton”, meaning that the point with the highest distance score to its cluster centre was assigned its own cluster. This forces the solution to always conform to the original cluster number. Generally, an empty cluster was produced in much less than 1 % of all the total iterative processes, so we do not consider this to have affected the overall result, especially since the k dependence of the solution quality was studied in any case.

The selection of cluster number k is unquestionably of high importance, as is the selection of the dissimilarity metric (Anderberg, 1973; Spath, 1980; Hastie et al., 2005), so they were more thoroughly and quantitatively investigated. Since the above-mentioned parameters were generally found to have a major effect on the clustering outcomes, they were not fixed, but kept as free parameters throughout the rest of the testing phase. This allowed us to observe whether the effects of preprocessing procedures would be dependent on k or the dissimilarity metric. The results of applying the commonly used preprocessing options, namely the intensity and mass scaling procedures recommended by Stein and Scott (1994), Horai and co-workers (2010), among others, are presented below.

3.2.2 Solution quality without preprocessing

Having no definitive preconception on the number of clusters, we evaluated clustering results for a range of k ($k = 2 \dots 20$) for all the metrics studied: squared Euclidean, city block/Manhattan, cosine and correlation. Using total solution silhouette value as a solution quality indicator, we search for the maxima (or clear elbows) in the silhouette results (Fig. 2), implying particularly favourable solutions.

Based on the silhouette value comparison for the unscaled data (Fig. 2) we conclude the following: the city block distance metric seems to perform poorly compared to the other three alternatives. The squared Euclidean, correlation and cosine methods are more or less equal in their silhouette quality, making the selection based on this test alone a difficult task. We also find the silhouette values for the latter methods between values of 0.25 and 0.50, suggested by Kaufman and Rousseeuw (1989) as a region of weak structure in the set of data, and calling for the use of additional methods to probe whether the implied structure is real or artificial. We additionally note that there is clear variation in silhouette values as a function of k , indicating a lower range ($k < 11$) solutions are more likely to correspond to natural divisions in the data than the high range ($k > 11$). In the following tests we therefore decided to include the range of $k = 2$ to $k = 12$.

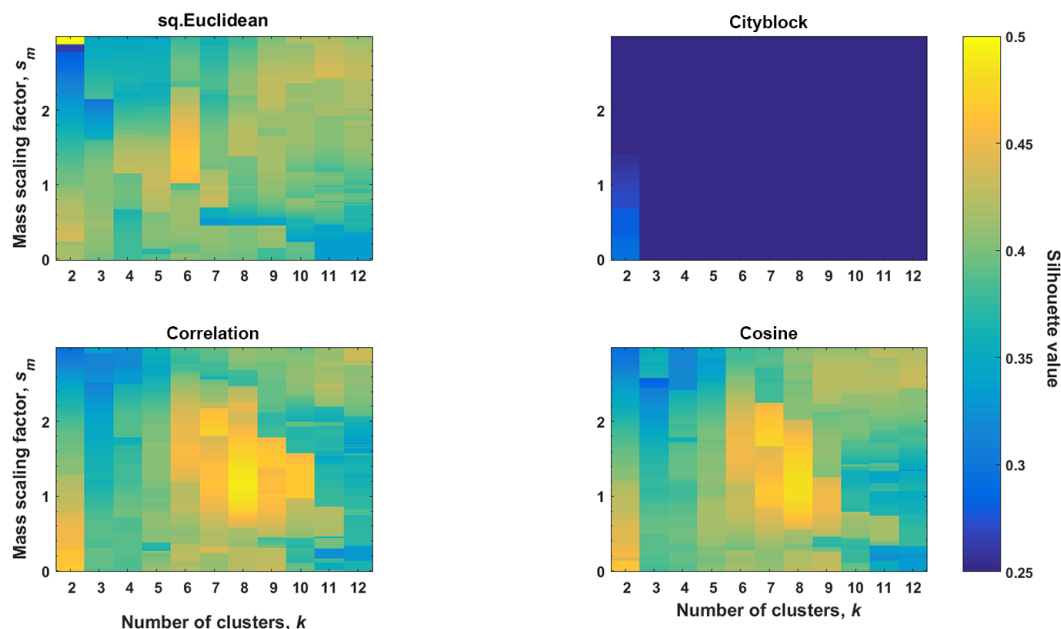


Figure 3. A contour plot for a field of solution silhouette values for the studied dissimilarity metrics, as a function of cluster size k (x axis) and mass scaling factor s_m (y axis). The maximum near-squared Euclidean $k = 2$, $s_m \approx 3$ indicate a solution with a high silhouette, but this solution only separates one outlier cluster ($n = 3$; cluster O-II, explained in the next section) from the other objects, so this solution was not considered separately.

For additional visualization, similar diagnostics for when (not specific metric optimization) mass scaling is applied are also presented in Fig. 2. The example mass scaling factor s_m of 1.36, selected for the briefly illustrating the effect from scaling, was selected based on a more comprehensive review presented below.

3.2.3 Solution quality with mass and intensity scaling

As preprocessing options we also tested the two methods recommended by Stein and Scott (1994), namely intensity and mass scaling of the data variables, as explained in Sect. 2.3.3, Eq. (10). Similar to Stein and Scott, we also explore values for s_i ranging from 1...2 and $s_m = 0...3$, with a step of 0.01 to pinpoint any maxima and evaluate the stability of the results with regard to minor changes in scaling values. The resulting 2-D field of solution silhouette values is shown in Fig. 3, and can be thought of as an extension to Fig. 2, which corresponds to the situation for scaling factors $s_m = 0$ and $s_i = 1$. Generally, the mass scaling processing was found to enhance the cluster-like structuring of the data, enabling improved differentiation between groups. It also seems there is no single value of s_m that would maximize the structure, but the optimum scaling factor value depends on the number of clusters (k). Even so, s_m values between 1 and 2 seem to produce the highest silhouette values for all metrics. If opting for the use of a single s_m value for similar AMS data, we therefore suggest, based on s_m distribution of solutions shown in Table 2, an s_m of 1.36 ± 0.24 (mean \pm SD) to be ex-

amined as a starting point. When comparing the scaled result silhouettes from non-preprocessed data, the improvement is non-homogeneous, and seems to specifically enhance some solutions over others, as illustrated in Fig. S7.

Similarly, intensity scaling was charted for $k = 2...12$ and $s_i = 0...3$. However, unlike mass scaling, intensity scaling only seems to deteriorate the solution quality for our AMS set of data, for the entire range of s_i values tested (0 to 1). The effect of intensity scaling is illustrated in Figs. S8 and S9. Based on this result, we would not recommend intensity scaling for a data set of this type without further results to the contrary.

Finally, we tested the combination of mass and intensity scaling, but found the results worse than for mass scaling alone. We additionally tested two methods with similar aims, namely omitting the low end mass spectrum < 45 Th and down-weighting m/z 44-related signals, similarly to the standard procedure in preprocessing PMF matrices, explained in Sect. 2.1.2. While omission of low masses seems to generally improve classification considerably (Sect. S3 and Fig. S1), we find the method too arbitrary to recommend, and find mass scaling can be used to produce similar results with better founded, more elegant methodology. The tests on m/z 44 down-weighting were inconclusive at best and would require further testing to be validated as a procedure with positive effects on clustering structure.

In conclusion of the preprocessing methods, we find mass scaling is the only method to consistently (but non-

Table 2. Diagnostics values, clustering parameters and cluster populations for solutions of 6 to 10 clusters. Oxidation level is described for each cluster centroid and potential sources are (preliminarily) identified. Within-cluster silhouette values are colour coded for readability (<0.24 orange, 0.25...0.49 yellow, >0.5 green). Solutions chosen for further analysis (correlation $k = 8$ and $k = 10$) are highlighted in red.

	s_m	k	silh	S-I INTERMEDIATE OXIDISED sawmill-SOA		S-II HIGHLY OXIDISED mixed anthropogenic		W-I INTERMEDIATE OXIDISED mixed anthropogenic		W-Ia INTERMEDIATE OXIDISED traffic (HOA)		W-Ib INTERMEDIATE OXIDISED cooking (COA)		W-Ic INTERMEDIATE OXIDISED biomass burning (BBOA)		W-II FRESH traffic (HOA)		W-III FRESH cooking COA (+BBOA?)		O-I OUTLIER (mz 58) amine source?		O-II OUTLIER (mz 100, mz 86) amine source?		O-III OUTLIER (mz 86) amine source?		
				n	silh	n	silh	n	silh	n	silh	n	silh	n	silh	n	silh	n	silh	n	silh	n	silh	n	silh	n
TOTAL SOLUTION																										
number of clusters																										
mass scaling optimisation																										
sqEucl	1.32	6	0.46	23	0.55	17	0.47	23	0.38							10	0.38			5	0.47	3	0.77			
Corr	1.62	6	0.45	23	0.66	17	0.51	21	0.30									11	0.33	6	0.15	3	0.90			
	1.23	7	0.46	23	0.65	17	0.57	15	0.25							9	0.41	8	0.35	6	0.08	3	0.86			
	1.21	8	0.48	23	0.65	17	0.56	15	0.25							9	0.41	8	0.35	5	0.48	3	0.86	1	N/A	
	1.42	9	0.46	21	0.65	16	0.53			12	0.34	7	0.32			10	0.33	6	0.16	5	0.49	3	0.89	1	N/A	
	1.36	10	0.46	21	0.64	16	0.54			11	0.35	6	0.28	3	0.17	9	0.37	6	0.23	5	0.49	3	0.88	1	N/A	
Cos	1.66	6	0.45	23	0.63	17	0.49	20	0.31							12	0.38			6	0.13	3	0.88			
	1.69	7	0.47	23	0.63	17	0.47	20	0.32							12	0.38			5	0.50	3	0.88	1	N/A	
	1.15	8	0.48	23	0.63	17	0.54	13	0.38							9	0.35	10	0.24	5	0.47	3	0.82	1	N/A	
	0.96	9	0.45	21	0.64	16	0.54			13	0.23	8	0.32			9	0.34	5	0.25	5	0.44	3	0.79	1	N/A	

homogeneously) enhance the data cluster structure. Whether the other procedures mentioned above might under certain circumstances or specific combinations also prove beneficial, is a question left for a more detailed future study. In the following, we will overview the silhouette maxima obtained using variable mass scaling, as presented in Fig. 3, and the information it reveals on the general structures within our set of data.

3.3 Overview of the clustering results

Having utilized the optimized parameters and preprocessing methods, based on the test results, we are yet left with a number of plausible solutions of almost equal mathematical quality. These solutions, shown as the bright silhouette maxima in Fig. 3, are connected to various structures in our set of pollution data. In the following we will try and interpret these data structures both from mathematical and physicochemical viewpoints.

Beginning with an overview of the favourable solutions of highest mathematical quality, we located and tabulated the maximum silhouette values obtainable for each dissimilarity metric and each number of clusters k . Examining the corresponding silhouette value distributions (Fig. S10), we set 0.45 as the prerequisite value for a solution to be included in this comparison. This translated to 12 solutions (i.e. maxima for the solution regions with silhouette >0.45) being selected for a detailed, manual examination and interpretation. The silhouettes of the top solutions and k are presented in Table 2.

A brief overview of the k values associated with highest silhouette solutions k (Fig. 3) suggest our set of objects would best be divided either in

- two distinct classes, emerging from the original data without any mass scaling, or
- a more complex classification leading to 6 to 10 separable classes when optimized mass scaling is applied.

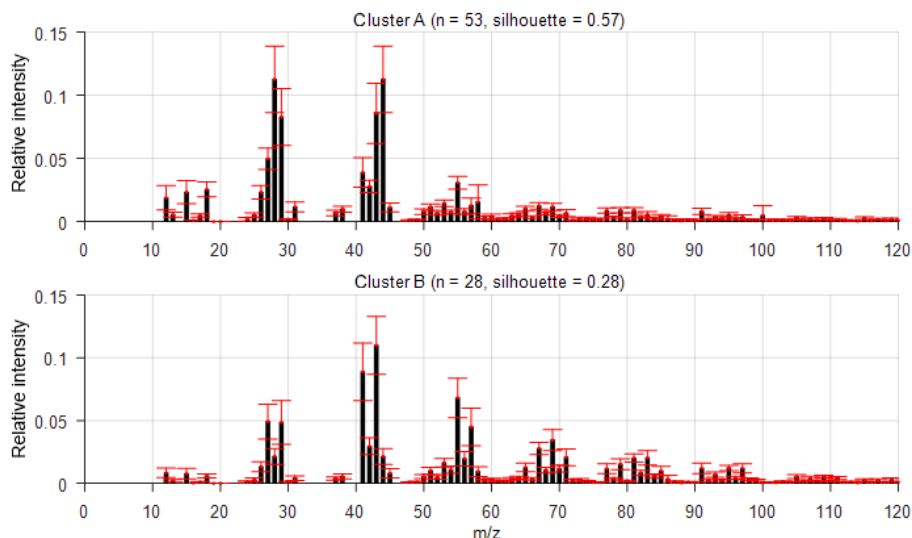


Figure 4. Weighted cluster centroid spectra for solution $k = 2$ (correlation and cosine) for the non-preprocessed data set. The $k = 2$ division appears to be driven mainly by age of the aerosol; cluster A corresponding to aged and cluster B to fresh aerosol. The error bars denote weighted within-cluster standard deviation.

We hypothesize that these alternative classifications correspond to different types of structures present in the data – a two-cluster structure would imply separation based on a dominant, binary-type variable, or a two-part division along a single axis (i.e. dimension, property), whereas 6 to 10 clusters likely imply divisions along more than one dimension. In the following we first investigate and interpret the binary (two-cluster) structure (Sect. 3.3.1), and subsequently aim to explain the finer, multidimensional structures and classifications reflected by the 6 to 10 cluster solutions (Sect. 3.3.2).

3.3.1 The two-cluster solution – separation by oxidation state

The two-cluster ($s_m = 0$) solutions, obtained with both cosine and correlation metrics, produce the exact same bicluster division of objects. To understand the reasoning of this separation, we need to examine the aerosol chemical differences between the two classes implied by the division. After constructing the mass spectra from weighted cluster centres (Fig. 4), we interpret the main chemical difference between the groups is the age (i.e. oxidation level) of the aerosol. Approximated oxygen-to-carbon (O:C) ratios can be calculated using Aiken’s “ambient” parameterization (Aiken et al., 2008) of

$$\text{O} : \text{C} (f_{44}) = 382 \times f_{44} + 00794, \quad (14)$$

where f_{44} is the fraction of total signal observed at 44 Th. This would yield an O:C of 0.51 for cluster A, branding it intermediately aged and semi-volatile (Canagaratna et al., 2015; Ng et al., 2010b), whereas cluster B’s O:C of 0.16 would imply it consists of fresh, hydrocarbon-dominated

aerosol pollution cases situated oxidation-wise somewhere between HOA and SV-OOA (Aiken et al., 2008; Jimenez et al., 2009; Ng et al., 2010b).

It should be noted that without mass scaling this separation is thus the most natural one (with silhouette maximum at $k = 2$; Fig. 2). The result is rather unsurprising considering the several low m/z (< 45 Th) oxidation-related signals (16 to 18, 29, 44 Th) usually dominating the signal fraction distributions. However, as the result also holds when down-weighting m/z 44 Th-derived signals, as mentioned in Sect. 3.2.3, we believe the two-factor solution is an actual, true structure in the data, as opposed to an artefact of the AMS fragmentation table calculations. We therefore conclude that the two-cluster structure represents aerosol classification into very fresh (cluster B) and relatively more aged (cluster A) groups.

3.3.2 Interpreting the underlying structures of higher order ($k = 6 \dots 10$) solutions

As the number of plausible solutions with similar magnitude (0.45 to 0.49) silhouettes for the preprocessed set of data is larger than just a few, we will not thoroughly describe all the solutions here or at this point claim one is superior to the others, but instead try to formulate a synthesis of the results, and identify the common features exhibited by the solutions.

When looking at all highest total silhouette values of the solutions, excluding the two-cluster solutions covered above and inspecting the mass spectra derived from the cluster centroids, we can find several analogous characteristics shared by essentially all the solutions. Presenting an overview of the $k = 6 \dots 10$ solutions in a tabular format (Table 2), we can begin to understand the underlying structures in com-

mon: firstly, there seem to be two ever-present, clear-cut clusters (silhouettes > 0.5) with high within-cluster silhouettes of 0.55...0.66 and 0.47...0.57, labelled here as strong clusters (S-I, S-II), with minor variations in cluster population size or the resulting centroid spectra.

Secondly, there seems to always be a group of two to three outlier clusters (O-I to O-III), each with very unique individual mass spectra. Here we brand them outlier groups due to their small cluster populations ($n = 1 \dots 6$) and the striking dissimilarity to other observed groups (additionally quantified in Table S1). While examining the changes in within-cluster silhouettes, we find the inclusion of the third, singleton outlier (O-III) in its own class a marked improvement to the solution in terms of cluster cohesion – a change also reflected in enhanced total solution quality when O-III is included.

The remaining clusters are much less pronounced (within-silhouettes typically < 0.4), and much less stable as k is increased – they clearly present the biggest challenge for this type of analysis. For the purposes of easy reference we term them the weak clusters (W-I to W-III).

Observing the composition of the weak clusters, they seem to form a structure independent to those of the clear-cut and outlier groups; the sum of population over the weak clusters is rather invariable ($n = 32 \dots 35$), and only in very few cases is there disagreement between the solutions in assigning an object into strong versus weak clusters. This potentially suggests the weak structure forms a supercluster distinct from both the strong and the outlier clusters. The inner cohesion of this supercluster, however, seems low, as evidenced by the low within-cluster silhouettes and the interchangeability in assignments into subclusters between equally good total solutions.

To examine the effect of outliers in data, we additionally excluded the outlier and/or the strong clustered objects and reran the analysis for the remaining data, but the results were found to revert to an analogous situation with the same problem of silhouette-wise ambiguity and low inner cohesion of the weak subclusters.

From examining the within-cluster silhouette values of the clusters we would be inclined to look primarily to the Table 2 solution at $k = 8$ for a correlation metric solution, due to the highest mathematical solution quality (silhouette 0.49) and reasonable (silhouette > 0.25) cohesion for all of the weak clusters. However, at this point we feel we have reached the limit of what we can conclude based on the silhouette values alone, and also have to consider the aerosol chemical interpretability of the solutions.

3.4 Aerosol chemical interpretation of clusters

As ever, when applying inherently mathematical algorithms such as PMF2/ME-2 and k -means++ to physical or chemical experimental data, it is important to remember the algorithms are, in the end, only analytical tools that in the best

case help in answering a particular question or gaining further understanding of the data. Their ultimate usefulness is, therefore, measured by the interpretability and applicability of the answer in the physical or chemical context, as much as its methodological robustness and statistical (un)certainty. In this work, the final test of our methodology is to see if we can understand the resulting cluster assignments in the context of aerosol chemistry and to interpret the clusters as air pollution types.

When interpreting aerosol mass spectra measured from ambient air, it should be kept in mind that the aerosol is not only the product of the primary emission or nucleation, but also the physicochemical processes taking place post-emission. These notably include condensation and evaporation of trace gases, as well as interaction with other aerosol types. In particular, it has been suggested that the interactions between the primary and secondary aerosols, and likewise anthropogenic and natural ones and their precursors, may play a considerable role in forming and transforming the atmospheric aerosols we observe (e.g. Weber et al., 2007; Carlton et al., 2010). These interactions are poorly understood and usually not taken into account when analysing ambient observations. It seems likely, though, that these effects would hinder attempts of classification by smearing out differences between aerosols from various different sources.

Also, the issues caused by collinearities in loadings (i.e. the inability of PMF to separate collocated single sources, but rather produce an extraction containing a linear combination of the single sources) may produce samples with inadequate deconvolution, which would exhibit a superposition of spectral features of many aerosol source types. In the clustering phase, these samples would be expected to show up as between-cluster objects, falling between the “pure” samples, and exhibiting low silhouette values. The posterior processing (Sect. 2.3.5) we applied should thus down-weight these mixed observations, diminishing their influence on the final cluster centroids. The collinearity problems caused by spectral profile similarities, on the other hand, are harder to resolve. In case of high similarities between spectral profiles from various combustion processes (hydrocarbon-like organic aerosol (HOA) vs. cooking organic aerosol (COA) vs. biomass burning organic aerosol (BBOA); Mohr et al., 2012) as well as the tendency for the most highly oxidized organized aerosols to closely resemble each other (Ng et al., 2010b; Zhang et al., 2011), the low dissimilarities between the objects hinder robust classification even if PMF manages to correctly extract these spectra from the background. In the end, differentiation between highly similar spectra comes down to the quality of (a) the classification algorithm, (b) the dissimilarity metric and (c) the data-weighting optimization. Although our algorithm selection was fixed in this work, the parameter optimizations described in Sect. 3.2 should provide us with an improved resolution for examining the aerosol chemical classes and structures in the set of data.

For AMS data we are fortunate to have access to years of research by the worldwide AMS users' community and the numerous studies reporting compositions of various aerosol types, which significantly helps us in understanding the cluster centroid spectra. An especially helpful information repository relevant for any AMS-related mass spectral identification and comparison exercises, such as the problem at hand, is the AMS spectral database (described by Ulbrich et al., 2009), containing a total of 248 unit resolution AMS spectra from both ambient air, chamber and combustion experiments. The spectra contain examples of source-attributed aerosol types obtained in laboratory experiments or ambient aerosol feature extraction, various averaged mass spectra of ambient aerosols over longer periods and laboratory standards measured using the AMS. As the spectra are obtained using many different AMS variants and under very different conditions, not all the spectra contain the same variables (m/z) or are normalized in a standard way, which may cause uncertainty when comparing spectra.

To help interpret our obtained clusters we calculated the similarities between the AMS spectral database specimens and the mass spectra derived from our cluster centroids. Where needed we would then refer to the specific publications describing the details of the comparison spectra of interest. As a measure of similarity we use the metric found to perform best for the tested data set (as per evaluation in Sect. 3.2), the Pearson product-moment correlation (Eq. 8), scaled dynamically by $(m/z)^{1.36}$. We believe to have shown mass scaling is advantageous also for measuring the similarity of AMS spectra, as it is well known to improve spectral similarity comparisons in mass spectrometric applications (e.g. Horai et al., 2010; Kim et al., 2012; Stein and Scott, 1994), and will thus use r_s and r_s^2 as measures of similarity between a pair of spectra instead of the uniformly weighted r and r^2 . Only correlations with $p < 0.05$ are considered.

As mentioned in Sect. 2.2, information on pollution event hourly times and peak wind directions was logged during the feature extraction analysis. The summary of these diagnostics sorted according to clustering results are shown in the Supplement (Sect. S9; Figs. S11, S12). However, due to the small number of objects in most clusters, sample sizes are too low for solid conclusions to be made from this auxiliary data.

3.4.1 The strong clusters – biomass burning and sawmill pollution

The clusters we can identify, quantify and interpret with high confidence are the strong clusters (S-I and S-II), clearly set apart by the k -means++ algorithm.

Looking at the correlations with database spectra, we find the first cluster (S-I) correlates highly ($r_s^2 = 0.85$) with the PMF-derived semi-volatile oxidized organic aerosol (SV-OOA) spectra reported by Ng et al. (2010a) as an average spectra of 15 ambient AMS data sets, and also correlates

with several other SV-OOA mass spectra from the database. The cluster S-I mass spectrum also correlates highly with most laboratory-generated boreal-forest-relevant secondary organic aerosols, e.g. those from α -terpinolene ($r_s^2 = 0.91$), α -terpinene (0.90), α -pinene (0.87), α -humulene (0.84) and myrcene (0.82) oxidation by ozone, reported by Bahreini et al. (2005). The spectrum also seems to closely match the biogenic background aerosol mass spectrum generally observed at the station when anthropogenic sources are absent. This type of spectrum has also been reported previously for the site, for example by Allan et al. (2006). As the strong plume-like nature of these air pollution events makes the possibility of a purely natural source for this aerosol type unlikely, we investigated the wind direction patterns during the peak concentration of the events classified in this category, along with the location of potential local and regional aerosol sources (Figs. S11, S13 to S16). Based on this auxiliary information, we conclude that the aerosol plumes likely originate from the nearby sawmills at Korkeakoski, situated some kilometres from the station, also matching the monoterpene plume observations of Liao et al. (2011). Despite the chemical similarity to natural semi-volatile background aerosol in boreal forest (e.g. OOA 2 from the work of Corrigan et al. (2013), the PMF model does manage to reliably discriminate the sawmill plume factor from the background, so it seems evident the two mass spectra have differences. We hence label this aerosol type the “sawmill secondary organic aerosol” (sawmill SOA), and hypothesize that it is formed via gas-to-particle conversion from the BVOCs emitted in large quantities as wood is cut and subsequently dried at the sawmills. Notable in this spectrum type is the almost complete lack of signal at 57 Th (corresponding to $C_4H_9^+$ and $C_3H_5O^+$; Mohr et al., 2012), a very typical peak to occur in most other anthropogenic AMS spectra.

The second cluster that can be easily identified is S-II. The absolutely highest correlation ($r_s^2 = 0.97$) within ambient spectra is the PMF-derived, aged, low-volatile biomass burning organic aerosol (OO2-BBOA) quantified by Crippa et al. (2013) for metropolitan Paris aerosol and with other similar, highly oxidized specimen, e.g. the low-volatile oxidized organic aerosol (LV-OOA; $r_s^2 = 0.93$) observed by Lanz et al. (2007a) in wintertime Zurich, and suggested in their analysis to have originated from wood burning. Of the laboratory spectra, it closely matches the spectra collected during a burning experiment for oak smouldering (Weimer et al., 2008; $r_s^2 = 0.85$) and burning a type of undergrowth vegetation (sage rabbit bush; $r_s^2 = 0.88$; Fire Lab at Missoula Experiment FLAME-1 – spectra submitted to AMS spectral database by J. Kroll). We name the S-II cluster “anthropogenic low-volatile oxidized organic aerosol” (A-LV-OOA) since, while it contains low numbers of biomass burning marker signals (m/z 60, $C_2H_4O_2^+$ and m/z 73 Th, $C_3H_5O_2^+$ fragments from the anhydrosugar levoglucosan; e.g. Elsasser et al., 2012; Cubison et al., 2011; Schneider et al., 2006), their ion concentrations remain low ($f_{60} + f_{73} < 0.01$) and

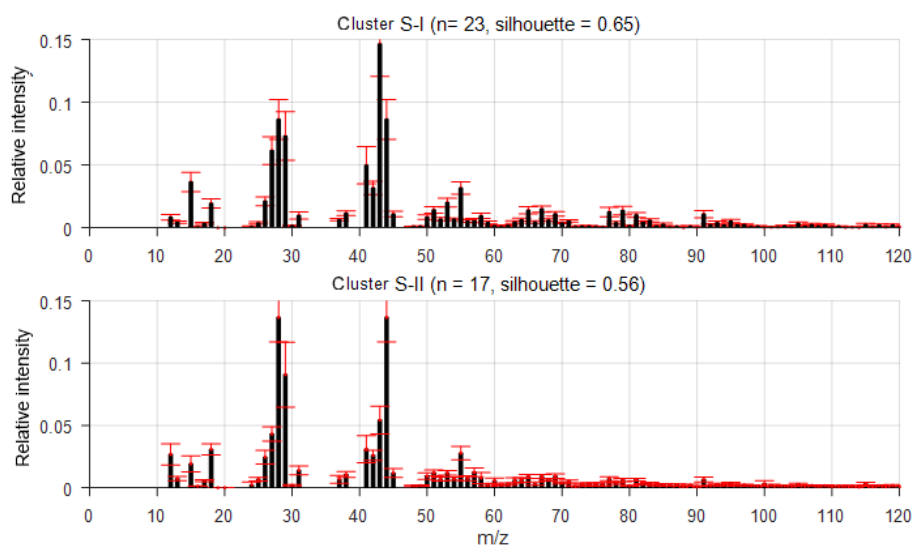


Figure 5. Mass spectra derived from [correlation, $k = 8$] clusters S-I (sawmill-SOA) and S-II (A-LV-OOA). Error bars indicate within-cluster variability (silhouette-weighted within-cluster standard deviation).

thus we are hesitant to say the aerosol is from biomass exclusively. As discussed in Sect. 2.2.1, despite limited population in the area, domestic wood burning is common in rural Finland for domestic heating during the cold season and recreational purposes (saunas, barbecues) during the warmer season, and it has been shown biomass burning smoke is rapidly oxidized upon release to the atmosphere (Hennigan et al., 2011; Cubison et al., 2011), producing low-volatile aerosol compounds in a matter of hours. It is also known (Ng et al., 2010b; Zhang et al., 2011) that upon reaching a high-level of oxidation, most aerosols start to resemble general LV-OOA, as they gradually lose their unique mass spectral features, making it plausible that the pollution aerosols in cluster S-II are from different sources. However, compared to the highly oxidized, biogenic background LV-OOA the S-II mass spectrum exhibits the m/z 57 and 60 Th anthropogenic markers and is missing the characteristic, large 53 Th peak generally reported in boreal forest biogenic background aerosol (e.g. OOA-1 reported by Corrigan et al., 2013). As the plume-like nature of the studied pollution episodes would also imply anthropogenic sources over natural ones, we conclude that S-II is almost certainly of anthropogenic origin.

The mass spectra of biomass burning and the sawmill aerosol groups, derived from the highest silhouette (0.49) solution (correlation, $k = 8$) are depicted in Fig. 5.

3.4.2 The weak clusters – anthropogenic fresh and semi-volatile aerosols from traffic, biomass burning, cooking and industry

Whether due to a very low number of observations, limits imposed by instrument SNR ratio, high chemical similarity between the weak clusters or inconclusively resolved PMF extractions due to plumes consisting of multiple sources,

the mass spectral structures separating the weak groups of aerosols from each other is much less pronounced than the division between the strong and the outlier cluster characteristic spectra relative to other aerosol types. Although it is hard to judge based on this set of data alone, we think the faults lie mostly with the collinearity issues arising from the chemical similarity and/or source collocation hypotheses, since the number of observations related to the weak groups overall is quite large (around 40 % of total) and the instrument SNR seems to enable the classification of other groups without ambiguity. From the general outlook of the weak clusters' spectra we observe many hints (low m/z 44 Th signal, pronounced 55 and 57 Th peaks, distinct repeating spectral structure at 65...83 Th) pointing to the direction of fresh anthropogenic combustion-originating aerosols.

The actual differentiation between AMS aerosol spectra from cooking, and traffic is notoriously hard for unit mass resolution spectra, as discussed by Mohr et al. (2012), and is traditionally mostly based on the relative abundances of signals at m/z 55 and 57 Th. Mass spectral differentiation between fresh BBOA and COA is even harder, as their characteristic unit-resolution spectra are near indistinguishable – we calculated a similarity of $r_s^2 = 0.83$ between (unit-resolution converted) COA and BBOA spectra from the data of Mohr et al. (2012). The nature of cooking fuel (e.g. wood, coal, natural gas) and use of cooking oil also likely affects the resulting COA spectrum and its similarity towards either HOA or BBOA.

Looking again at the highest silhouette solution (correlation, $k = 8$), the fresh aerosol types with the lowest O : C are clusters W-II (O : C = 0.15) and W-III (0.15). Cluster W-II translates to a characteristic spectra that best correlates with hydrocarbon-like organic aerosol (HOA) reported by

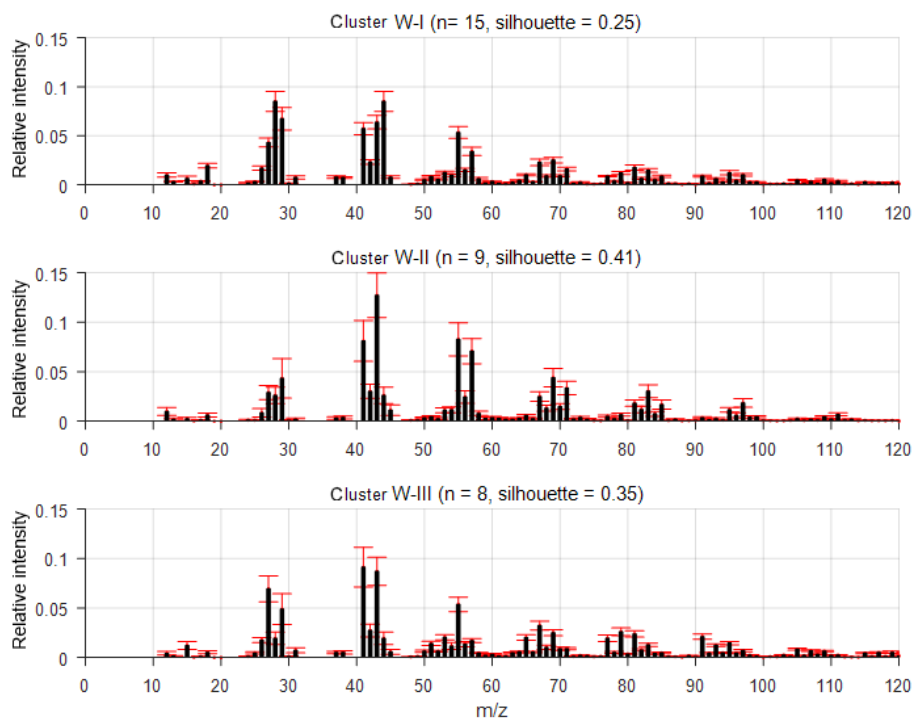


Figure 6. Mass spectra corresponding to clusters W-I (A-SV-OOA), W-II (HOA) and W-III (COA). Error bars denote within-cluster variability (silhouette-weighted within-cluster standard deviation). Solution for correlation $k = 8$.

Ulbrich et al. (2009; for Pittsburgh), Crippa et al. (2013; Paris), Lanz et al. (2007a; Zurich), and the average HOA of 15 data sets described by Ng et al. (2010b) with respective r_s^2 's of 0.92, 0.91, 0.90 and 0.92. Similarities with laboratory data are observed with aerosol specimen such as lubricating oil aerosol ($r_s^2 = 0.87$), diesel bus exhaust (0.90) and fuel (0.77), reported by Canagaratna et al. (2004), but notably high similarity also exist with mass spectra from burning plastic (0.96) and the aerosol products of various cooking experiments ($r_s^2 = 0.84 \dots 0.92$), described by Mohr et al. (2009), as well as laboratory spectra of decanal (0.86) and hexadecanol (0.84) measured by Alfarra et al. (2004). However, the similarities of W-II spectra to reputable cooking organic aerosol spectra, extracted from comparable ambient observations (e.g. Mohr et al., 2012; Crippa et al., 2013) are notably lower (0.62; 0.71), compared to the aforementioned indications that this aerosol class would be related to traffic-related HOA. The ratio of m/z 55 : m/z 57 signals for this aerosol type is 1.17, agreeing with findings by Mohr et al. (2012) for HOA.

The wind direction analysis combined with a potential source survey (available in Sect. S9; Figs. S11, S13 to S16) additionally points to the conclusion that the source of this aerosol is in the sector with a nearby public road. We thus term W-II as hydrocarbon-like organic aerosol (HOA) in accordance with AMS aerosol naming conventions.

The other “fresh” aerosol type, W-III (Fig. 3.6) exhibits highest similarities ($r_s^2 = 0.88, 0.86$) with the aforemen-

tioned ambient cooking aerosols, measured in Barcelona (Mohr et al., 2012) and Paris (Crippa et al., 2013) while correlating markedly less (0.53...0.72) with the HOA spectra of the database. Laboratory spectrum matches are with charbroiling (0.72; Lanz et al., 2007a) β -caryophyllene (0.87) and β -pinene (0.75; Bahreini et al., 2005), the former sesquiterpene being an important constituent in many essential plant oils used in cooking. Moderate correlations ($r_s^2 = 0.56 \dots 0.70$) are found with Mohr et al. (2012) cooking aerosol specimen and the various smoke chamber spectra from FLAME-1 (0.36...0.79) mass spectra (Fire Lab at Missoula Experiment – spectra submitted to AMS spectral database by J. Kroll). Signal ratio m/z 55 : m/z 57 for the W-III spectrum is 3.14, which, when interpreted in accordance with the COA estimation method introduced by Mohr et al. (2012), suggests this aerosol type would be cooking related. We therefore label the W-III cluster as cooking organic aerosol (COA). However, in the end, due to the close similarity of COA and BBOA (Mohr et al., 2012), we cannot rule out the possibility of fresh biomass burning or combustion aerosol from barbecues also contributing to this mixed class of observations.

Separating both of these fresh two subclasses from the weak supercluster leaves us with the semi-volatiles species in the form of one to three clusters. The solution with one semi-volatile aerosol pollution type, W-I, in (correlation, $k = 8$) is mathematically the most robust one.

W-I pollution type exhibits mixed mass spectral characteristics between the HOA and COA types (Fig. 6). The main difference with the former two-cluster spectra is the spectra from the remaining part of the weak cluster (W-X) group implies a considerably higher oxidation state (estimated O : C ratio of 0.40 compared to 0.18 and 0.15 for HOA and COA; Aiken et al., 2008; Eq. 14). The library spectra similarity examination brands this aerosol a general semi-volatile oxidized organic aerosol (SV-OOA), with the closest similarity to SV-OOA observed in Barcelona ($r_s^2 = 0.91$; Mohr et al., 2012) and Pasadena ($r_s^2 = 0.88$; Hersey et al., 2011). The similarities to ambient urban aerosols, HOA and COA, as well as traffic-, burning- and cooking-related laboratory spectra, are generally moderate to high (typically 0.5...0.8) but with no real pointers to a single, dominant type of origin over the others. The ratio of m/z 55 : m/z 57 of 1.57 is between that of the HOA (1.17) and COA (3.14) spectra (Mohr et al., 2012) and the higher m/z range (45 to 100 Th) seem to offer little in terms of features distinct from COA and HOA. We brand W-III a A-SV-OOA, for anthropogenic semi-volatile oxidized organic aerosol, to separate it from the biogenic and natural SV-OOA types, such as semi-volatile forest background or sawmill-SOA aerosols, as the close connection to combustion-related aerosol types seems evident based on the (dis)similarities between the clusters. We hypothesize that this aerosol type is a mixture of anthropogenic aerosols from various origins, such as traffic, cooking and possibly industrial processes, the common feature of which is that they have been subjected to some oxidation and mixing, smearing out the characteristic features of more distinct classes of aerosols such as the fresh HOA and COA types.

However, we will also present an on-going interpretation based on the $k = 10$ (correlation) solution with three separate A-SV-OOA factors: we suggest these three classes could be interpreted as source-specific anthropogenic SV-OOA types. We hypothesize that the differences between the fresh aerosol types, sorted according to their emission source, are not yet completely smeared out by an intermediate level of oxidation. This would allow k -means++ to differentiate (albeit with much less confidence) between the A-SV-OOA types, resulting in differentiation based on origin either from traffic SV(HOA), cooking SV(COA) or biomass burning SV(BBOA), shown in Fig. 7.

This interpretation is indeed supported to some extent by the correlation examination against HOA, COA and BBOA spectra of the AMS spectral database (Table S3 in the Supplement), and in the case of SV(HOA), the only group with a moderate number of observations ($n = 11$), also by the wind direction analysis, pointing to the south-to-west sector with the main nearby roads as the sector of origin (Figs. S11 and S13). To corroborate this finer source specific differentiation of A-SV-OOA, however, a larger amount of observations would certainly be beneficial.

3.4.3 The outliers – amine compounds from biogenic sources?

While the spectra examined thus far seem interpretable in the “traditional” framework of AMS aerosol-type classification (LV-OOA, SV-OOA, BBOA, HOA, COA), the outlier clusters do not fit these conventional categories. There are also no spectra matching our observations in the AMS spectral library. We therefore additionally examine the spectral features and compare them to observations in other mass spectrometry literature.

To begin with, we note the distinctive feature of all the mass spectra outlier clusters are rather “exotic”, at least in an AMS context, with peaks at 58, (72), 86 and 100 Th (Fig. 8). These even molecular masses are relatively rarely observed in the AMS organic spectra due to the nitrogen rule implying the presence of a nitrogen atom. The homologous ion series of amine compounds ($C_nH_{2n+2}N^+$) yields masses 30, 44, 58, 72, 86, 100 Th (Kraj et al., 2008), exactly matching the peaks not obscured by other large ions, which suggests the presence of various amine compounds.

Ge et al. (2011) calculated in their review article a grand total of 67 aerosol phase amine observations (1972–2009). Amine spectra with some similar features have been observed elsewhere (Aiken et al., 2009; Huffman et al., 2009; Sun et al., 2011; Chang et al., 2011), and amines have been postulated to contribute to the AMS organic signal at 30 Th at the SMEAR II station (Allan et al., 2006). None of the studies cited offer a close match, however, and many of the main spectral features and signal ratios differ markedly from the ones seen here. Additionally, some rather similar spectra have been presented by Murphy et al. (2007), who measured secondary aerosol generated from various aliphatic amines using an AMS, and the 70 eV electron impact ionization spectrum of trimethylamine, available from the US National Institute of Standards and Technology (NIST).

The aerosol phase amine sources have thus far mostly been attributed to either local industrial pollution or marine biological production (see Ge et al., 2011 for a review of observations). In our case both of these sources would be surprising considering the inland location and the scarcity of nearby industrial plants, along with the apparent seasonal dependence of the observations (only observed in the springtime measurements). However, we cannot rule them out at this point. As additional hypotheses for the origin we offer the following: (1) biodegradation-produced volatile aerosol precursors released at snowmelt (Kieloaho et al., 2013; Kuhn et al., 2011), (2) manure application to agricultural fields or amine emissions from nearby cattle farm (Schade and Crutzen, 1995; Ge et al., 2011; Kuhn et al. 2011; Sintermann et al., 2014; Sect. S12, Fig. S14) and (3) biogenic amine emissions (Kieloaho et al., 2013) related to clear-cutting a nearby patch of forest (Virkkula et al., 2014).

An additional discussion on the amines and their potential origins is available in the Supplement (Sect. S12). This

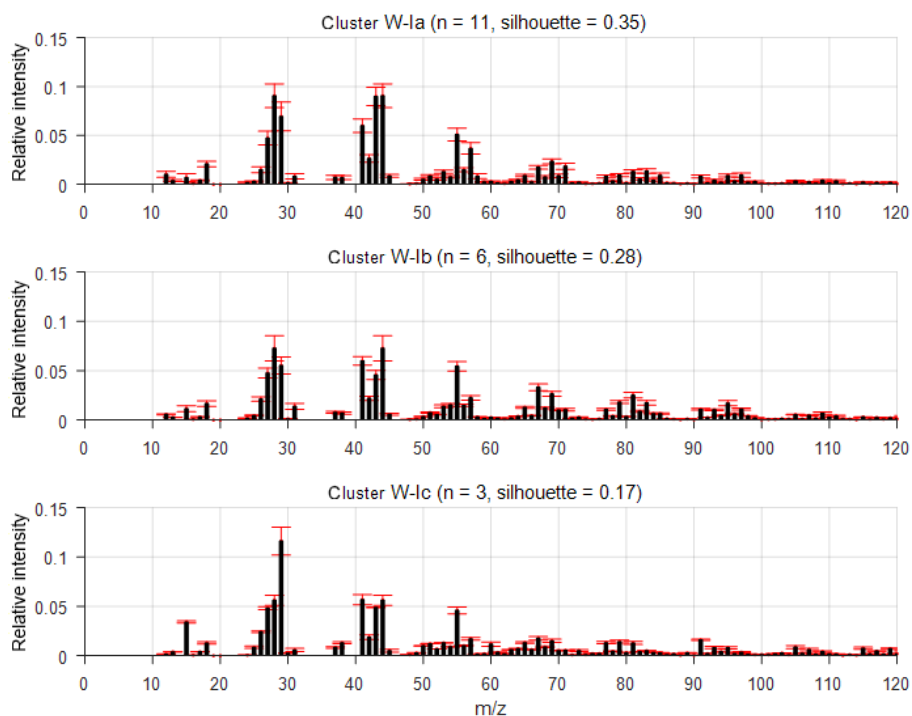


Figure 7. Mass spectra for the correlation $k = 10$ solution, dividing the intermediate oxidized objects into three groups, labelled here, according to their proposed sources, as W-Ia (SV(HOA)), W-Ib (SV(COA)) and W-Ic (SV(BBOA)). Error bars represent within-cluster variability (silhouette-weighted within-cluster standard deviation).

section also includes a discussion on alternative sources for these signals and, while the final decision on the sources and origins of the outlier clusters' spectra remains speculative, we believe the most likely explanation is the amine compounds. Therefore we name the outlier I-III peaks “amine-58” (O-I), “amine-100” (O-II) and “amine-86” (O-III) with respect to their major characteristic peaks, most likely corresponding to fragment ions with elemental composition CH_4N^+ (at m/z 30 Th), $\text{C}_2\text{H}_6\text{N}^+$ (44 Th), $\text{C}_3\text{H}_8\text{N}^+$ (58 Th), $\text{C}_4\text{H}_{10}\text{N}^+$ (72 Th), $\text{C}_5\text{H}_{12}\text{N}^+$ (86 Th) and $\text{C}_6\text{H}_{14}\text{N}^+$ (at 100 Th).

3.5 Interpretation of spectral structures and main dimensions defining the pollution types

Below we try to summarize what we consider the most important dimensions or axes, on which the more complex ($k = 6 \dots 10$) classifications would be based, and their interpretation in an aerosol chemical framework.

3.5.1 Oxidation level and aerosol age

Traditional AMS spectral analysis revolves around studying the process of oxidation or the ageing of an aerosol particle in the atmosphere. The oxidation process depends on particle chemical structure, number and type of oxidant radicals available and the time spent in the atmosphere, so it is highly variable and difficult to model. From this branch

of study and the connection of volatility to oxidation level (Donahue et al., 2011, 2012; Kroll et al., 2011; Jimenez et al., 2009), some of the “standard” labels for atmospheric processed aerosol types (LV-OOA, SV-OOA) also originate. It has been known for a long time in the AMS community that mass spectra peaks such as m/z 43 Th (C_3H_7^+ fragment from alkyl group molecules and $\text{C}_2\text{H}_3\text{O}^+$ from non-acid organic oxidation products; e.g. Ng et al., 2011) and 44 Th (CO_2^+ ; common fragment from carboxylic acids; Duplissy et al., 2011), as well as their relative contributions, are good indicators of oxidation (Aiken et al., 2007; Ng et al., 2011; Canagaratna et al., 2015). Upon ageing, the fraction of organic aerosol signal observed at 44 Th (f_{44}) and O : C ratio of a particle increase, and the marker for fresh emissions, m/z 43 Th signal goes down along with most high mass (>45 Th) signals. Agreeing with the clear separation of aerosol types by age found in the clustering solutions of this work, the “oxidation axis” is clearly one of the main dimensions along which cluster borders are drawn.

3.5.2 Aerosol source-specific characteristics

The other axes for cluster separation seem to relate to their source-specific fingerprints. The results presented in Sect. 3.1 and 3.2, and particularly the solution diagnostics values shown in Table 2, suggest that there are one or more source-related divisions resulting in a fairly clear-cut separation

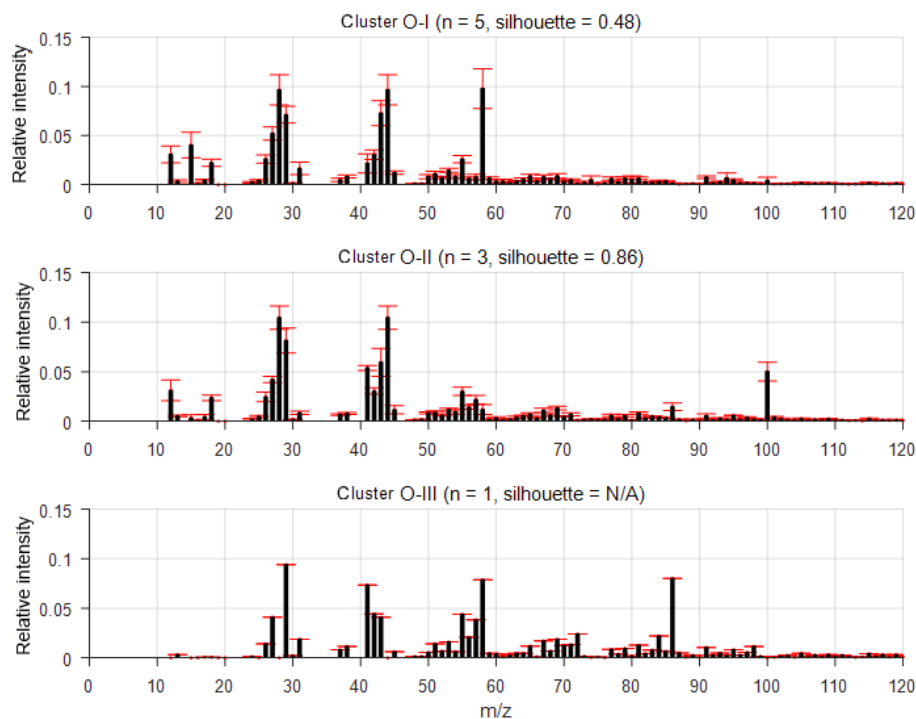


Figure 8. Mass spectra corresponding to weighted cluster centroids (correlation, $k = 8$) for groups O-I (amine-58), O-II (amine-100) and O-III (amine-86). Error bars denote within-cluster variability (silhouette-weighted within-cluster standard deviation, unavailable for the singleton O-III).

ration of clusters. One such clear division seems to be between the anthropogenic aerosol groups considered primary, and thus usually originated from a combustion process (such as biomass or fossil fuel burning, combustion engines exhaust or aerosol formed in high-temperature cooking), and the secondary aerosol from particle conversion biogenic organic vapours (albeit in our case from anthropogenic sources in the form of the sawmills). In our case this distinction separates the sawmill secondary organic aerosol (cluster S-I) from other aerosols of similar age and oxidation from different sources (especially W-I) in a clear-cut manner. A short examination on a potential S-I spectral marker at m/z 53 Th can be found in the Supplement (Sect. S11, Fig. S17).

The structure that is the most difficult to explain conclusively is the set of mass spectral features setting apart the various components of the observed weak cluster structure. The separation of fresh HOA from COA and BBOA has been discussed and characterized in many studies (e.g. Crippa et al., 2013; Mohr et al., 2009), but in practise classifying these aerosols in an unambiguous manner remains troublesome. It does, however, seem clear from the results presented here that the $f_{55} : f_{57}$ ratio is indeed a viable indicator of a dimension separating HOA pollution type (low $f_{55} : f_{57}$) from COA and BBOA, as suggested by e.g. Mohr et al. (2009) and Crippa et al. (2013). We note the $f_{55} : f_{57}$ values derived from the clustering solution, 1.17 for HOA

and 3.14 for COA, match well with the estimates given by Mohr (0.9 ± 0.2 for HOA; 3.0 ± 0.7 for COA). Furthermore, there also appear to be additional, equally definitive indicators available in the higher masses, as discussed in the Supplement (Sect. S11; Fig. S18).

As the important separation of the sawmill-SOA cluster (S-I) also happens to be clearly reflected in the $f_{55} : f_{57}$ dimension, due to the very low f_{57} signal in its centroid mass spectrum, we adopt this axis selection along with the oxidation axis (reflected by estimated O : C) as a basis for representing the clustering solution in a simplified way. This results in a two-dimensional projection of the 125-dimensional data structure (Fig. 9). It should be underlined that this representation is a crude simplification of the actual solution, aimed at providing at least some visualization of the tremendously more complex spatial structure. Consequently, many of the potentially more complex structures located higher up on the m/z scale equally driving the solution are not shown, which explains why some points seem to be out of place in the two-dimensional projection. With that said, the solution does seem to make a lot of sense, and we can see that the clusters are relatively well defined.

For this set of observations we did not obtain a separate distinct (fresh) BBOA cluster, so we were unable to evaluate the difference between BBOA and COA. As for the more controversial classification of A-SV-OOA subtypes, the sep-

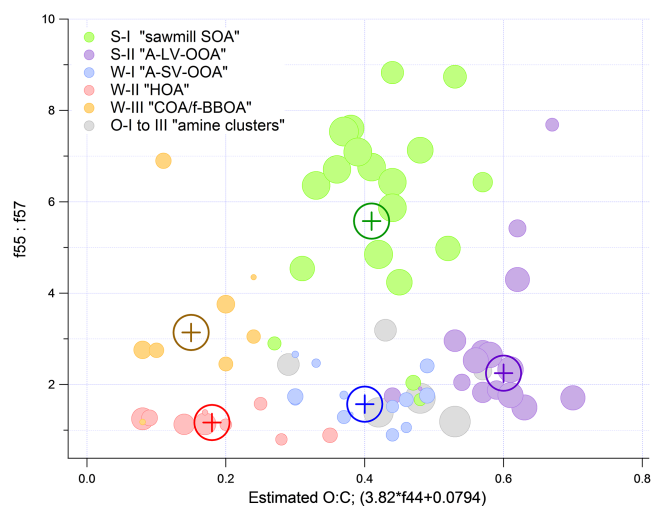


Figure 9. Correlation $k = 8$ clustering solution projected onto 2-D axes, corresponding to f_{44} derived oxidation level (estimated O:C; Aiken et al., 2008) and $f_{55} : f_{57}$ ratio (truncated at 10) typically used for COA vs. HOA source apportionment (Mohr et al., 2012). Marker size corresponds to silhouette value of the point, ranging from zero to one. Cluster centroid locations are marked separately with darker colours. Outlier clusters are shown in grey, without centroids.

aration can be visualized in the $(f_{55} : f_{57}, f_{60} + f_{73})$ space (Fig. 10), f_{60} and f_{73} corresponding to the expected biomass burning axis (Cubison et al., 2011; Elsasser et al., 2012; Schneider et al., 2006). The low cohesion of A-SV(COA) and A-SV(BBOA) clusters in particular is likely due to both (a) very few observations available and (b) a scarcity of clear mass spectral differences between the groups.

3.5.3 Exotic variables specific to outlier observations and groups

In addition to these more traditional fingerprints in the AMS spectra, in this case we also have outlier observations, distinguishable by their unusual high mass (m/z 58, [76], 86, 100 Th) signals. It seems evident the dimension separating these groups would correspond to these specific variables. This reasoning is also supported by visualization of the outlier spectra (Fig. 11) in an appropriate 2-D space (e.g. $f_{86} + f_{100}$ vs. f_{58}).

3.6 Estimating the natural variability within the aerosol types

Finally, we briefly examine the intracluster variabilities, translating to inferred mass spectral variability within the aerosol types. While we feel it would be dangerous to claim that the variation within the spectra of a specific group can be directly understood as the natural variability of that aerosol type at this site, we propose it can be considered as an upper limit estimate of this variability, since the within-cluster

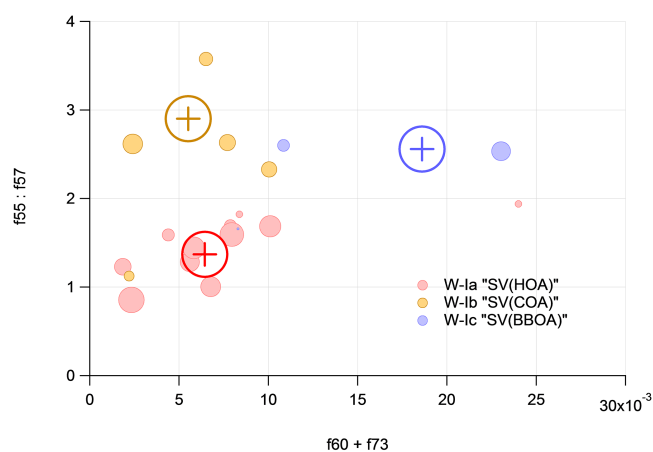


Figure 10. Classification of A-SV-OOA (Cluster W-I) types into subgroups W-Ia, W-Ib and W-Ic, corresponding to SV(HOA), SV(COA) and SV(BBOA). 2-D visualization is given in y axis f_{55}/f_{57} (truncated to 4) and x axis $f_{60} + f_{73}$. Marker size indicates object silhouette value. Other groups (W-II, W-III, S-X, O-X) are omitted from graph. Due to small sample size and low cohesion of clusters such a classification should be considered speculative at this point.

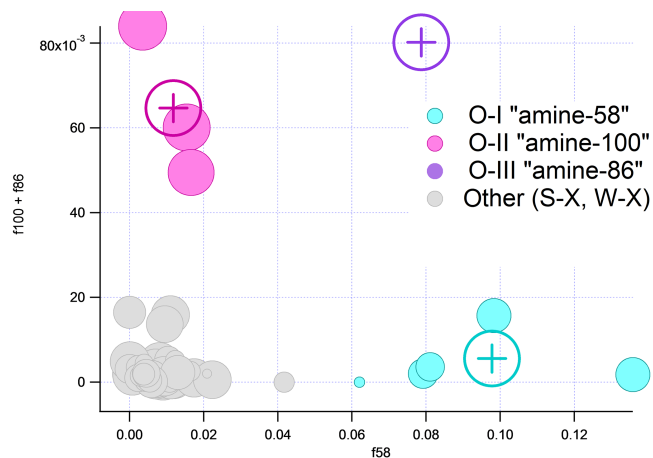


Figure 11. Outlier clusters (O-I to O-III) assumed to contain amines, and their respective centroids plotted in colour, and any other clusters in grey in $(f_{58}, f_{86} + f_{100})$ spatial projection. Marker size corresponds to object silhouette value (unavailable for the singleton cluster O-III).

variation is caused both by the actual variability in the natural aerosol, and the uncertainty induced by its measurement and analysis. Overall, the effects of instrument (white) noise is filtered in the feature extraction (PMF) phase, and the effects of possible misclassifications or presence of mixed source pollution events (collocated sources incompletely resolved by PMF) in clustering are likely limited to borderline, between cluster cases that have minimal influence on the final spectra due to the silhouette-based posteriori weighting. The collinearity effects discussed in Sect. 2.3.1 do contribute

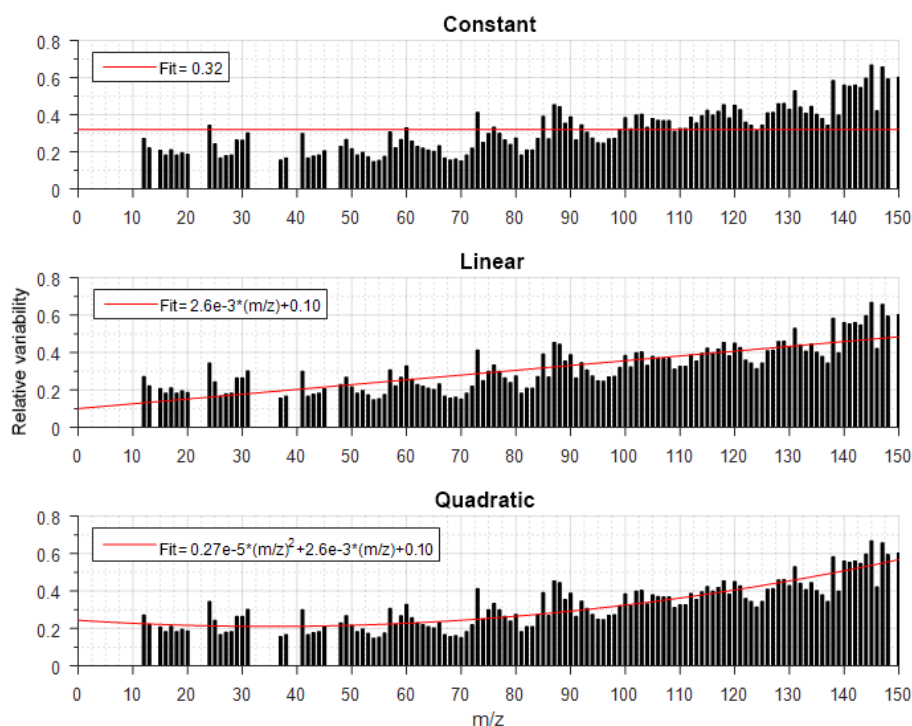


Figure 12. Silhouette-weighted standard deviation, as a function of m/z , for cluster S-I (sawmill-SOA). Upper panel: constant value (a value) estimate. Middle panel: linear regression estimate. Lower panel: exponential (quadratic) regression estimate.

to the total analysis error, but their quantitative determination was not achieved in this work. For the clean-cut, high-silhouette strong and outlier clusters collinearity is unlikely to introduce significant uncertainty, and the analysis uncertainties would be expected to afflict mostly the weak clusters more susceptible to source collocation and high spectral similarities. However, such a distinct difference seems absent between the estimated variabilities of strong and weak clusters, lending confidence that the collinearity effect is not consequential for this set of data. The rotational ambiguity of PMF remains an issue, and while we have done our best to find the cleanest possible separation of the pollution and background spectra, some degree of uncertainty is unavoidable. Although there some tools have been proposed to assess the rotational sensitivity (e.g. bootstrapping; Norris et al., 2008; Tibshirani et al., 2001), the exact level of mass spectral uncertainty arising from the rotational ambiguity remains difficult to quantify. Also as the standard k -means does not utilize information of uncertainties of input objects, a profound error analysis would require more advanced classification tools. We note the uncertainty estimates of PMF results is a topic still requiring attention, as highlighted by Reff et al. (2007), and the field of AMS PMF would likely benefit from development of further easy-to-approach statistical tools. Nevertheless, considering there exist very few if any statistically well-founded estimates for this type of aerosol variability, we propose that in the absence of more reliable results, the variabilities im-

plied by this study can be used as an indicator of the likely magnitude of the underlying natural variability within the observed classes of aerosols at a site like this.

We examined the within-cluster variabilities of the aerosol types studied, and calculated silhouette-weighted standard deviations as a function of m/z ratio, which was then fitted with constant, linear and exponential (quadratic) regression models. An example of such a parameterization is shown in Fig. 12, and the model parameters for all clusters (in the correlation $k = 8$ solution) are given in Table 3.

The variability parameters are especially important for (partially or fully) constrained factor analysis, such as techniques utilizing the ME-2 algorithm. For example, in the most commonly approach used in the Source Finder (SoFi), a single value (a value; Canonaco et al., 2013), it is typical to restrict allowed spectral variation to a certain fraction of the reference spectra, applied uniformly across all m/z ratios. Based on this work we find that the a value approach may not be the optimal way to restrict spectral variation allowed in factorization models such as the ME-2-driven constrained PMF, and that m/z dependent parameterizations would better represent the actual natural variability that should be accommodated by the model. Ultimately, pulling approaches (Canonaco et al., 2013; Paatero and Hopke, 2009) might prove preferable to hard limit constraints for variation. Nevertheless, if still opting for the use of a constant a value, our results imply the natural variability within an aerosol type

Table 3. Within-cluster, silhouette-weighted variabilities parameterized using constant, linear and exponential (quadratic) least squares regressions to the clustered data (variability [y] as a function of m/z [x]). The constant variability estimate corresponds to the a value approach used in ME-2 analysis for constraining the PMF model.

Cluster		Constant	Linear fit		Quadratic fit		
		$y = a$	$y = bx + a$		$y = cx^2 + bx + a$		
		a	b (10^{-3})	a	c (10^{-5})	b (10^{-3})	a
S-I	sawmill SOA	0.32	2.56	0.10	2.70	-1.89	0.24
S-II	A-LV-OOA	0.34	1.81	0.19	1.60	-0.82	0.27
W-I	A-SV-OOA	0.18	0.59	0.13	1.28	-1.51	0.19
W-II	HOA	0.41	1.60	0.28	5.37	-7.25	0.56
W-III	COA	0.24	-0.09	0.24	3.25	-5.44	0.41

may be significantly larger than what is often allowed in conjunction with the constrained PMF/ME-2 (e.g. Crippa et al., 2014).

4 Conclusions

While advanced data analytical techniques, such as PMF, have already been widely adopted for AMS data reduction and feature extraction, the application of similar chemometric methods for AMS spectra identification and classification is as of yet an uncommon sight.

In this study we make a pitch for adopting some of the tried and tested statistical methods from other mass spectrometric fields into the analysis of AMS results. As a practical example we present a case of applying simple clustering to a set of AMS pollution spectra, and show that even a simple algorithm such as the k -means++ can, with proper optimization, match and reproduce the traditional expert classification of AMS aerosol types unsupervised (i.e. without a priori training).

Clustering as a method is especially sensitive to certain parameters; the algorithm used, data preprocessing (scaling) and the dissimilarity measure (distance metric) used for the objects' spatial representation. In this work we compared the performance of some of the most basic measures of dissimilarity in k -means++ clustering for our example data, along with some suggested data preprocessing (scaling) methods. At least in the context of this limited case, the [Pearson] correlation metric seems slightly preferential as a measure of spectral (dis)similarity, closely followed by [dot product] cosine and squared Euclidean dissimilarity measures – at least when the AMS mass spectra are normalized. For representing spectral similarity of unnormalized data, we suggest either cosine or correlation metrics due to mathematical considerations (i.e. multiplication invariance).

Optimized mass scaling, that is, weighting the mass spectra signals by an exponential function of their m/z ratios, seems beneficial for unsupervised classification of AMS aerosol types. Based on our example set of data we suggest scaling the signal variables at each mass-to-charge by

an exponential weight $(m/z)^{s_m}$ of $s_m = 1.36 \pm 0.24$. Contrarily, intensity scaling, or scaling the MS variables (signals) by their root function appears to be detrimental for the structure of our spectral data set. We hypothesize that this may be due to our spectra being normalized to unity and generally not being overtly dominated by any individual signals – unlike spectra in many soft ionization MS applications – potentially upscaling general instrument noise more than the informative minor signals.

Without scaling as a preprocessing step, k -means++ produces a differentiation between oxidized and fresh(er) aerosol samples. Up-weighting higher m/z signals allows for classification in the framework of source-specific AMS organic aerosol subcategories such as differentiating between HOA and COA, strongly indicating that much of the information needed for this classification resides among the higher up m/z variables. We thus suggest taking this piece of information into consideration when interpreting and classifying AMS spectra, either manually or by applying a machine-learning approach. Exploring similar mass scaling in connection with comparable statistical analysis methods may prove useful, especially in applications where data weighting is already commonplace and easy to implement.

Limiting the role of PMF to solving short-term air pollution events and plumes with minimal number of factors facilitates identification of the physically meaningful rotation, which best temporally separates the pollution plume from the background aerosol. Using correlation minimum between the time series of the pollution and the background as a selection criterion minimizes the need for expert judgement by human analysts when exploring PMF solutions of pollution events. Similarly, applying computer-aided, unsupervised classification, any result should be more or less free of analyst bias when deciding the classifications of mass spectra to organic aerosol subtypes. An appropriately chosen clustering quality metric, such as the silhouette value, can be used to infer the natural number of clusters in data as well as to optimize scaling factors, to magnify the structures present in data. Naturally, this does not excuse the human analyst from the final responsibility of physicochemical interpretation, compar-

ison and evaluation of the mathematical solutions produced by any classification algorithm. It should also be noted that the first phases of the task, of manually identifying pollution events and performing the feature extraction step for each of the events individually, is very labour-intensive and some subjectivity remains in deciding the selection criteria for what constitutes a pollution episode – hence the process should ideally be made more automatic and statistics based.

Despite the laboriousness, compared to currently used approaches such as trying to use PMF to directly extract source-specific, anthropogenic organic aerosol subtypes from extended data sets and identify the correct rotations from the resulting solution space, we suggest the methodology presented here has several advantages. (1) Due to limiting the PMF time windows to short pollution episodes explained with fewer factors and variability driven by pollution plume behaviour, the major factor analytical problem of rotational ambiguity is diminished and there is less need for expert judgement in the selection of solutions. Concentrating on short-lived events also better fulfils the factor analytical receptor model's assumption of constant profiles (i.e. aerosol bulk composition is not driven by chemical processes but a result mixing from different sources). (2) From the clustering solution it is possible to derive solid, quantitative estimates of the archetypal pollution spectra along with their uncertainties – information which has direct use and value when applying the reference spectra in e.g. constraining future factor analyses. Detailed chemical knowledge on pollution types may also help in further understanding the physicochemical properties of anthropogenic atmospheric aerosols and their interactions. Finally, (3) by analysing air pollution cases individually we can also identify and extract minor sources and identify outlier aerosol types, which fall way under the PMF's limit of detection, of explaining approximately 5% of the variability of the total aerosol mass (Ulbrich et al., 2009). These outlier groups may ultimately prove important and offer new scientific information, as exemplified by the observation of suspected amine compounds presented in our results.

In our example of applying feature extraction (PMF) and unsupervised classification (*k*-means++) to a set of AMS data, we could produce reference spectra and their variability estimates for local pollution archetypes. Aerosol chemical interpretation of the results from our test bed set of data from a background, boreal forest station (SMEAR II) suggests that the main dimensions or “axes” driving the classification relate to (a) an oxidation state reflecting aerosol ageing; (b) source types, whether representing spectral structures of various combustion source types (traffic, cooking, biomass burning) or characteristics of aerosol formed from biogenics through gas-to-particle conversion; (c) exotic variables characteristic of outlier observations and outlier groups (from the perspective of traditional AMS aerosols' classifications). We observe that although atmospheric ageing does gradually smear out the characteristics of the emitted aerosols, statistically resolvable spectral features seem to be retained and

could be used to infer the origin of the emission. However, as the spectral similarity of aerosols increases, a proper selection of dissimilarity metric and scaling becomes essential, as does the availability of a sufficient amount of high-precision observations of single-component pollution plumes. In future studies we also suggest exploring soft classification algorithms, such as fuzzy clustering (Dunn et al., 1973), in connection with aerosol mass spectral classification to avoid potential issues with non-discrete or incompletely deconvolved samples.

We propose that optimizing the similarity metrics, both via correctly selecting the algorithm and data weighting, provides not only a basis for exploratory classification but also a means for identifying AMS spectra by comparing them with references available in the AMS spectral database. We can also see prospective use for exploratory classification, with clustering as an obvious example, in evaluating sets of discrete or deconvolved AMS spectral samples, such as the samples often produced in large numbers in bootstrapping or sensitivity analysis exercises when evaluating factor analytical models.

Ultimately, we hope to have demonstrated that statistics-based, computer-aided classification of AMS spectra seems promising, and in that the differences and characteristic features of mass spectra can indeed be parameterized for an increasingly machine-learning-oriented approach to AMS advanced data analysis.

5 Data availability

Data used are available upon request from the authors. Cluster centroid spectra will be made available in the AMS Spectral Database (<http://cires1.colorado.edu/jimenez-group/AMSsd/>) upon publication, and the individual spectra extracted from the air pollution events along with their classification are also available online (at <https://etsin.avointiede.fi/dataset/urn-nbn-fi-csc-kata20170118173805948017>; Äijälä et al., 2017).

The Supplement related to this article is available online at doi:10.5194/acp-17-3165-2017-supplement.

Competing interests. The authors declare that they have no conflict of interest.

Acknowledgements. We acknowledge the funding from the following programmes: European Commission FP6 projects EUCAARI (036833-2), FP7 ACTRIS (262254), the Horizon 2020 project ACTRIS-2 (654109), ERC Grant COALA (638703), the Finnish COE project CRAICC (272041) and the Academy of Finland COE in Atmospheric Science (2008–2019).

We wish to thank the Hyttiälä and Helsinki technical staff (Pasi Aalto, Erkki Siivola, Frans Korhonen, Heikki Laakso, Toivo Pohja, Veijo Hiltunen and Janne Levula) for support with experimental measurements and the AMS users' community for valuable feedback on the data analytical topics.

The authors are grateful for the comments and suggestions provided by the anonymous referees for improving the manuscript.

Edited by: D. Spracklen

Reviewed by: two anonymous referees

References

- Aalto, P., Hameri, K., Becker, E., Weber, R., Salm, J., Makela, J. M., Hoell, C., O'Dowd, C. D., Karlsson, H., Hansson, H. C., Vakeva, M., Koponen, I. K., Buzorius, G., and Kulmala, M.: Physical characterization of aerosol particles during nucleation events, *Tellus B*, 53, 344–358, doi:10.1034/j.1600-0889.2001.530403.x, 2001.
- Aiken, A. C., DeCarlo, P. F., and Jimenez, J. L.: Elemental analysis of organic species with electron ionization high-resolution mass spectrometry, *Anal. Chem.*, 79, 8350–8358, 2007.
- Aiken, A. C., Decarlo, P. F., Kroll, J. H., Worsnop, D. R., Huffman, J. A., Docherty, K. S., Ulbrich, I. M., Mohr, C., Kimmel, J. R., Sueper, D., Sun, Y., Zhang, Q., Trimborn, A., Northway, M., Ziemann, P. J., Canagaratna, M. R., Onasch, T. B., Alfarra, M. R., Prevot, A. S., Dommen, J., Duplissy, J., Metzger, A., Baltensperger, U., and Jimenez, J. L.: O/C and OM/OC ratios of primary, secondary, and ambient organic aerosols with high-resolution time-of-flight aerosol mass spectrometry, *Environ. Sci. Technol.*, 42, 4478–4485, 2008.
- Aiken, A. C., Salcedo, D., Cubison, M. J., Huffman, J. A., DeCarlo, P. F., Ulbrich, I. M., Docherty, K. S., Sueper, D., Kimmel, J. R., Worsnop, D. R., Trimborn, A., Northway, M., Stone, E. A., Schauer, J. J., Volkamer, R. M., Fortner, E., de Foy, B., Wang, J., Laskin, A., Shutthanandan, V., Zheng, J., Zhang, R., Gaffney, J., Marley, N. A., Paredes-Miranda, G., Arnott, W. P., Molina, L. T., Sosa, G., and Jimenez, J. L.: Mexico City aerosol analysis during MILAGRO using high resolution aerosol mass spectrometry at the urban supersite (T0) – Part 1: Fine particle composition and organic source apportionment, *Atmos. Chem. Phys.*, 9, 6633–6653, doi:10.5194/acp-9-6633-2009, 2009.
- Äijälä, M., Junninen, H., Petäjä, T., Kulmala, M., Worsnop, D., and Ehn, M.: De-convolved mass spectra from the air pollution events and their classification solution, available at: <https://etsin.avointiede.fi/dataset/urn-nbn-fi-csc-kata20170118173805948017> (last access: 20 February 2017), 2017.
- Alfarra, M. R., Coe, H., Allan, J. D., Bower, K. N., Boudries, H., Canagaratna, M. R., Jimenez, J. L., Jayne, J. T., Garforth, A. A., Li, S. M., and Worsnop, D. R.: Characterization of urban and rural organic particulate in the lower Fraser valley using two aerodyne aerosol mass spectrometers, *Atmos. Environ.*, 38, 5745–5758, doi:10.1016/j.atmosenv.2004.01.054, 2004.
- Allan, J. D., Jimenez, J. L., Williams, P. I., Alfarra, M. R., Bower, K. N., Jayne, J. T., Coe, H., and Worsnop, D. R.: Quantitative sampling using an Aerodyne aerosol mass spectrometer 1. Techniques of data interpretation and error analysis, *J. Geophys. Res.-Atmos.*, 108, 4090, doi:10.1029/2002JD002358, 2003.
- Allan, J. D., Alfarra, M. R., Bower, K. N., Coe, H., Jayne, J. T., Worsnop, D. R., Aalto, P. P., Kulmala, M., Hyötyläinen, T., Cavalli, F., and Laaksonen, A.: Size and composition measurements of background aerosol and new particle growth in a Finnish forest during QUEST 2 using an Aerodyne Aerosol Mass Spectrometer, *Atmos. Chem. Phys.*, 6, 315–327, doi:10.5194/acp-6-315-2006, 2006.
- Anderberg, M. R.: Cluster analysis for applications, Monographs and textbooks on probability and mathematical statistics, in: Academic Press, Inc., New York, 1973.
- Anderson, T. W.: An Introduction to Multivariate Statistical Analysis, 2nd Edn., Wiley, New York, 1984.
- Arthur, D. and Vassilvitskii, S.: *k*-means++: The advantages of careful seeding, Proceedings of the eighteenth annual ACM-SIAM symposium on Discrete algorithms, 1027–1035, 2007.
- Ausloos, P., Clifton, C., Lias, S., Mikaya, A., Stein, S., Tchekhovskoi, D., Sparkman, O., Zaikin, V., and Zhu, D.: The critical evaluation of a comprehensive mass spectral library, *J. Am. Soc. Mass Spectr.*, 10, 287–299, 1999.
- Bahreini, R., Keywood, M., Ng, N., Varutbangkul, V., Gao, S., Flagan, R., Seinfeld, J., Worsnop, D., and Jimenez, J.: Measurements of secondary organic aerosol from oxidation of cycloalkenes, terpenes, and m-xylene using an Aerodyne aerosol mass spectrometer, *Environ. Sci. Technol.*, 39, 5674–5688, 2005.
- Ball, G. H. and Hall, D. J.: ISODATA, a novel method of data analysis and pattern classification, DTIC Document, 1965.
- Belis, C., Karagulian, F., Larsen, B., and Hopke, P.: Critical review and meta-analysis of ambient particulate matter source apportionment using receptor models in Europe, *Atmos. Environ.*, 69, 94–108, 2013.
- Belu, A. M., Graham, D. J., and Castner, D. G.: Time-of-flight secondary ion mass spectrometry: techniques and applications for the characterization of biomaterial surfaces, *Biomaterials*, 24, 3635–3653, doi:10.1016/S0142-9612(03)00159-5, 2003.
- Caliński, T. and Harabasz, J.: A dendrite method for cluster analysis, *Commun. Stat.-Theor. M.*, 3, 1–27, 1974.
- Canagaratna, M. R., Jayne, J. T., Ghertner, D. A., Herndon, S., Shi, Q., Jimenez, J. L., Silva, P. J., Williams, P., Lanni, T., Drewnick, F., Demerjian, K. L., Kolb, C. E., and Worsnop, D. R.: Chase studies of particulate emissions from in-use New York City vehicles, *Aerosol Sci. Tech.*, 38, 555–573, doi:10.1080/02786820490465504, 2004.
- Canagaratna, M. R., Jayne, J. T., Jimenez, J. L., Allan, J. D., Alfarra, M. R., Zhang, Q., Onasch, T. B., Drewnick, F., Coe, H., Middlebrook, A., Delia, A., Williams, L. R., Trimborn, A. M., Northway, M. J., DeCarlo, P. F., Kolb, C. E., Davidovits, P., and Worsnop, D. R.: Chemical and microphysical characterization of ambient aerosols with the aerodyne aerosol mass spectrometer, *Mass Spectrom. Rev.*, 26, 185–222, doi:10.1002/mas.20115, 2007.
- Canagaratna, M. R., Jimenez, J., Kroll, J., Chen, Q., Kessler, S., Massoli, P., Hildebrandt Ruiz, L., Fortner, E., Williams, L., and Wilson, K.: Elemental ratio measurements of organic compounds using aerosol mass spectrometry: characterization, improved calibration, and implications, *Atmos. Chem. Phys.*, 15, 253–272, doi:10.5194/acp-15-253-2015, 2015.

- Canonaco, F., Crippa, M., Slowik, J. G., Baltensperger, U., and Prévôt, A. S. H.: SoFi, an IGOR-based interface for the efficient use of the generalized multilinear engine (ME-2) for the source apportionment: ME-2 application to aerosol mass spectrometer data, *Atmos. Meas. Tech.*, 6, 3649–3661, doi:10.5194/amt-6-3649-2013, 2013.
- Carlton, A. G., Pinder, R. W., Bhave, P. V., and Pouliot, G. A.: To what extent can biogenic SOA be controlled?, *Environ. Sci. Technol.*, 44, 3376–3380, 2010.
- Carmichael, J. W. and Sneath, P. H.: Taxometric maps, *Syst. Biol.*, 18, 402–415, 1969.
- Chang, R. Y.-W., Leck, C., Graus, M., Müller, M., Paatero, J., Burkhardt, J. F., Stohl, A., Orr, L. H., Hayden, K., Li, S.-M., Hansel, A., Tjernström, M., Leaitch, W. R., and Abbatt, J. P. D.: Aerosol composition and sources in the central Arctic Ocean during ASCOS, *Atmos. Chem. Phys.*, 11, 10619–10636, doi:10.5194/acp-11-10619-2011, 2011.
- Cormack, R. M.: A review of classification, *J. R. Stat. Soc. Ser. A-G.*, 134, 321–367, 1971.
- Corrigan, A., Russell, L., Takahama, S., Äijälä, M., Ehn, M., Junninen, H., Rinne, J., Petäjä, T., Kulmala, M., and Vogel, A.: Biogenic and biomass burning organic aerosol in a boreal forest at Hyttiälä, Finland, during HUMPPA-COPEC 2010, *Atmos. Chem. Phys.*, 13, 12233–12256, doi:10.5194/acp-13-12233-2013, 2013.
- Crippa, M., DeCarlo, P., Slowik, J., Mohr, C., Heringa, M., Chirico, R., Poulain, L., Freutel, F., Sciare, J., and Cozic, J.: Wintertime aerosol chemical composition and source apportionment of the organic fraction in the metropolitan area of Paris, *Atmos. Chem. Phys.*, 13, 961–981, doi:10.5194/acp-13-961-2013, 2013.
- Crippa, M., Canonaco, F., Lanz, V., Äijälä, M., Allan, J., Carbone, S., Capes, G., Ceburnis, D., Dall'Osto, M., and Day, D.: Organic aerosol components derived from 25 AMS data sets across Europe using a consistent ME-2 based source apportionment approach, *Atmos. Chem. Phys.*, 14, 6159–6176, doi:10.5194/acp-14-6159-2014, 2014.
- Cubison, M., Ortega, A., Hayes, P., Farmer, D., Day, D., Lechner, M., Brune, W., Apel, E., Diskin, G., and Fisher, J.: Effects of aging on organic aerosol from open biomass burning smoke in aircraft and laboratory studies, *Atmos. Chem. Phys.*, 11, 12049–12064, doi:10.5194/acp-11-12049-2011, 2011.
- Davies, D. L. and Bouldin, D. W.: A cluster separation measure, *IEEE T. Pattern Anal.*, 1, 224–227, 1979.
- DeCarlo, P. F., Kimmel, J. R., Trimborn, A., Northway, M. J., Jayne, J. T., Aiken, A. C., Gonin, M., Fuhrer, K., Horvath, T., Docherty, K. S., Worsnop, D. R., and Jimenez, J. L.: Field-deployable, high-resolution, time-of-flight aerosol mass spectrometer, *Anal. Chem.*, 78, 8281–8289, doi:10.1021/ac061249n, 2006.
- Docherty, K. S., Aiken, A. C., Huffman, J. A., Ulbrich, I. M., DeCarlo, P. F., Sueper, D., Worsnop, D. R., Snyder, D. C., Peltier, R., and Weber, R.: The 2005 Study of Organic Aerosols at Riverside (SOAR-1): instrumental intercomparisons and fine particle composition, *Atmos. Chem. Phys.*, 11, 12387–12420, doi:10.5194/acp-11-12387-2011, 2011.
- Donahue, N. M., Epstein, S. A., Pandis, S. N., and Robinson, A. L.: A two-dimensional volatility basis set: 1. organic-aerosol mixing thermodynamics, *Atmos. Chem. Phys.*, 11, 3303–3318, doi:10.5194/acp-11-3303-2011, 2011.
- Donahue, N. M., Kroll, J., Pandis, S. N., and Robinson, A. L.: A two-dimensional volatility basis set – Part 2: Diagnostics of organic-aerosol evolution, *Atmos. Chem. Phys.*, 12, 615–634, doi:10.5194/acp-12-615-2012, 2012.
- Drewnick, F., Hings, S. S., DeCarlo, P., Jayne, J. T., Gonin, M., Fuhrer, K., Weimer, S., Jimenez, J. L., Demerjian, K. L., Borrmann, S., and Worsnop, D. R.: A new time-of-flight aerosol mass spectrometer (TOF-AMS) – Instrument description and first field deployment, *Aerosol Sci. Tech.*, 39, 637–658, doi:10.1080/02786820500182040, 2005.
- Drewnick, F., Hings, S. S., Alfarra, M. R., Prevot, A. S. H., and Borrmann, S.: Aerosol quantification with the Aerodyne Aerosol Mass Spectrometer: detection limits and ionizer background effects, *Atmos. Meas. Tech.*, 2, 33–46, doi:10.5194/amt-2-33-2009, 2009.
- Dunn J. C.: A Fuzzy Relative of the ISODATA Process and its Use in Detecting Compact, Well Separated Clusters, *J. Cybernetics*, 3, 32–57, 1974.
- Duplissy, J., DeCarlo, P. F., Dommen, J., Alfarra, M. R., Metzger, A., Barmapadimos, I., Prevot, A. S., Weingartner, E., Tritscher, T., and Gysel, M.: Relating hygroscopicity and composition of organic aerosol particulate matter, *Atmos. Chem. Phys.*, 11, 1155–1165, doi:10.5194/acp-11-1155-2011, 2011.
- Eerdekens, G., Yassaa, N., Sinha, V., Aalto, P., Aufmhoff, H., Arnold, F., Fiedler, V., Kulmala, M., and Williams, J.: VOC measurements within a boreal forest during spring 2005: on the occurrence of elevated monoterpene concentrations during night time intense particle concentration events, *Atmos. Chem. Phys.*, 9, 8331–8350, doi:10.5194/acp-9-8331-2009, 2009.
- Elsasser, M., Crippa, M., Orasche, J., DeCarlo, P., Oster, M., Pitz, M., Cyrys, J., Gustafson, T., Pettersson, J. B., and Schnelle-Kreis, J.: Organic molecular markers and signature from wood combustion particles in winter ambient aerosols: aerosol mass spectrometer (AMS) and high time-resolved GC-MS measurements in Augsburg, Germany, *Atmos. Chem. Phys.*, 12, 6113–6128, doi:10.5194/acp-12-6113-2012, 2012.
- Farmer, D., Matsunaga, A., Docherty, K., Surratt, J., Seinfeld, J., Ziemann, P., and Jimenez, J.: Response of an aerosol mass spectrometer to organonitrates and organosulfates and implications for atmospheric chemistry, *P. Natl. Acad. Sci. USA*, 107, 6670–6675, 2010.
- Fortier, J. and Solomon, H.: Clustering procedures, *Multivariate analysis*, 1966.
- Freutel, F., Drewnick, F., Schneider, J., Klimach, T., and Borrmann, S.: Quantitative single-particle analysis with the Aerodyne aerosol mass spectrometer: development of a new classification algorithm and its application to field data, *Atmos. Meas. Tech.*, 6, 3131–3145, doi:10.5194/amt-6-3131-2013, 2013.
- Gauss, C.-F.: *Theoria combinationis observationum erroribus minimis obnoxiae*, Gottingae, Henricus Dieterich 1823, Henricus Dieterich, 1823.
- Ge, X., Wexler, A. S., and Clegg, S. L.: Atmospheric amines – Part I, A review, *Atmos. Environ.*, 45, 524–546, 2011.
- Gordon, A. D.: *Classification*, Chapman & Hall/CRC Monographs on Statistics & Applied Probability, 1999.
- Griffiths, J.: A brief history of mass spectrometry, *Anal. Chem.*, 80, 5678–5683, 2008.

- Hansen, A., Rosen, H., and Novakov, T.: The aethalometer – an instrument for the real-time measurement of optical absorption by aerosol particles, *Sci. Total Environ.*, 36, 191–196, 1984.
- Hari, P. and Kulmala, M.: Station for measuring ecosystem-atmosphere relations, *Boreal Environ. Res.*, 10, 315–322, 2005.
- Hastie, T., Tibshirani, R., Friedman, J., and Franklin, J.: The elements of statistical learning: data mining, inference and prediction, *Math. Intell.*, 27, 83–85, 2005.
- Hennigan, C., Miracolo, M., Engelhart, G., May, A., Presto, A., Lee, T., Sullivan, A., McMeeking, G., Coe, H., and Wold, C.: Chemical and physical transformations of organic aerosol from the photo-oxidation of open biomass burning emissions in an environmental chamber, *Atmos. Chem. Phys.*, 11, 7669–7686, doi:10.5194/acp-11-7669-2011, 2011.
- Henry, R. C.: Current factor analysis receptor models are ill-posed, *Atmos. Environ.*, 21, 1815–1820, 1987.
- Henry, R. C., Lewis, C. W., Hopke, P. K., and Williamson, H. J.: Review of receptor model fundamentals, *Atmos. Environ.*, 18, 1507–1515, 1984.
- Hersey, S., Craven, J., Schilling, K., Metcalf, A., Sorooshian, A., Chan, M., Flagan, R., and Seinfeld, J.: The Pasadena Aerosol Characterization Observatory (PACO): chemical and physical analysis of the Western Los Angeles basin aerosol, *Atmos. Chem. Phys.*, 11, 7417–7443, doi:10.5194/acp-11-7417-2011, 2011.
- Hings, S. S., Walter, S., Schneider, J., Borrmann, S., and Drewnick, F.: Comparison of a quadrupole and a time-of-flight aerosol mass spectrometer during the Feldberg aerosol characterization experiment 2004, *Aerosol Sci. Tech.*, 41, 679–691, 2007.
- Hopke, P. K.: Review of receptor modeling methods for source apportionment, *J. Air Waste Manage.*, 66, 237–259, 2016.
- Horai, H., Arita, M., Kanaya, S., Nihei, Y., Ikeda, T., Suwa, K., Ojima, Y., Tanaka, K., Tanaka, S., Aoshima, K., Oda, Y., Kakazu, Y., Kusano, M., Tohge, T., Matsuda, F., Sawada, Y., Hirai, M. Y., Nakanishi, H., Ikeda, K., Akimoto, N., Maoka, T., Takahashi, H., Ara, T., Sakurai, N., Suzuki, H., Shibata, D., Neumann, S., Iida, T., Tanaka, K., Funatsu, K., Matsuura, F., Soga, T., Taguchi, R., Saito, K., and Nishioka, T.: MassBank: a public repository for sharing mass spectral data for life sciences, *J. Mass. Spectrom.*, 45, 703–714, doi:10.1002/jms.1777, 2010.
- Hotelling, H.: Analysis of a complex of statistical variables into principal components, *J. Educ. Psychol.*, 24, 417–441, 1933.
- Huffman, J. A., Jayne, J. T., Drewnick, F., Aiken, A. C., Onasch, T., Worsnop, D. R., and Jimenez, J. L.: Design, modeling, optimization, and experimental tests of a particle beam width probe for the aerodyne aerosol mass spectrometer, *Aerosol Sci. Tech.*, 39, 1143–1163, 2005.
- Huffman, J. A., Docherty, K. S., Aiken, A. C., Cubison, M. J., Ulbrich, I. M., DeCarlo, P. F., Sueper, D., Jayne, J. T., Worsnop, D. R., Ziemann, P. J., and Jimenez, J. L.: Chemically-resolved aerosol volatility measurements from two megacity field studies, *Atmos. Chem. Phys.*, 9, 7161–7182, doi:10.5194/acp-9-7161-2009, 2009.
- Jimenez, J. L., Canagaratna, M. R., Donahue, N. M., Prevot, A. S., Zhang, Q., Kroll, J. H., DeCarlo, P. F., Allan, J. D., Coe, H., Ng, N. L., Aiken, A. C., Docherty, K. S., Ulbrich, I. M., Grieshop, A. P., Robinson, A. L., Duplissy, J., Smith, J. D., Wilson, K. R., Lanz, V. A., Hueglin, C., Sun, Y. L., Tian, J., Laaksonen, A., Raatikainen, T., Rautiainen, J., Vaattovaara, P., Ehn, M., Kulmala, M., Tomlinson, J. M., Collins, D. R., Cubison, M. J., Dunlea, E. J., Huffman, J. A., Onasch, T. B., Alfarra, M. R., Williams, P. I., Bower, K., Kondo, Y., Schneider, J., Drewnick, F., Borrmann, S., Weimer, S., Demerjian, K., Salcedo, D., Cottrell, L., Griffin, R., Takami, A., Miyoshi, T., Hatakeyama, S., Shimojo, A., Sun, J. Y., Zhang, Y. M., Dzepina, K., Kimmel, J. R., Sueper, D., Jayne, J. T., Herndon, S. C., Trimborn, A. M., Williams, L. R., Wood, E. C., Middlebrook, A. M., Kolb, C. E., Baltensperger, U., and Worsnop, D. R.: Evolution of organic aerosols in the atmosphere, *Science*, 326, 1525–1529, doi:10.1126/science.1180353, 2009.
- Jimenez, J. L., Jayne, J. T., Shi, Q., Kolb, C. E., Worsnop, D. R., Yourshaw, I., Seinfeld, J. H., Flagan, R. C., Zhang, X. F., Smith, K. A., Morris, J. W., and Davidovits, P.: Ambient aerosol sampling using the Aerodyne Aerosol Mass Spectrometer, *J. Geophys. Res.-Atmos.*, 108, 8425, doi:10.1029/2001jd001213, 2003.
- Johnson, R. L. and Wall, D. D.: Cluster Analysis of Semantic Differential Data I, *Educ. Psychol. Meas.*, 29, 769–780, 1969.
- Jolliffe, I.: Introduction, in: *Principal Component Analysis*, Springer, 1–7, 1986.
- Karoui, R., Downey, G., and Blecker, C.: Mid-infrared spectroscopy coupled with chemometrics: A tool for the analysis of intact food systems and the exploration of their molecular structure – Quality relationships – A review, *Chem. Rev.*, 110, 6144–6168, 2010.
- Kaufman, L. and Rousseeuw, P. J.: Finding groups in data: an introduction to cluster analysis, John Wiley & Sons, 2009.
- Kell, D. B.: Metabolomics and systems biology: making sense of the soup, *Curr. Opin. Microbiol.*, 7, 296–307, 2004.
- Kieloaho, A.-J., Hellén, H., Hakola, H., Manninen, H. E., Nieminen, T., Kulmala, M., and Pihlatie, M.: Gas-phase alkylamines in a boreal Scots pine forest air, *Atmos. Environ.*, 80, 369–377, 2013.
- Kim, S., Koo, I., Wei, X., and Zhang, X.: A method of finding optimal weight factors for compound identification in gas chromatography–mass spectrometry, *Bioinformatics*, 28, 1158–1163, 2012.
- Kowalski, B. R.: Analytical chemistry as an information science, *TrAC Trends, Anal. Chem.*, 1, 71–74, 1981.
- Kraj, A., Desiderio, D. M., and Nibbering, N. M.: Mass spectrometry: instrumentation, interpretation, and applications, John Wiley & Sons, 2008.
- Kroll, J. H., Donahue, N. M., Jimenez, J. L., Kessler, S. H., Canagaratna, M. R., Wilson, K. R., Altieri, K. E., Mazzoleni, L. R., Wozniak, A. S., Bluhm, H., Mysak, E. R., Smith, J. D., Kolb, C. E., and Worsnop, D. R.: Carbon oxidation state as a metric for describing the chemistry of atmospheric organic aerosol, *Nat. Chem.*, 3, 133–139, doi:10.1038/Nchem.948, 2011.
- Kuhn, U., Sintermann, J., Spirig, C., Jocher, M., Ammann, C., and Neftel, A.: Basic biogenic aerosol precursors: Agricultural source attribution of volatile amines revised, *Geophys. Res. Lett.*, 38, 16811, doi:10.1029/2011gl047958, 2011.
- Kulmala, M., Rannik, Ü., Pirjola, L., Dal Maso, M., Karimäki, J., Asmi, A., Jäppinen, A., Karhu, V., Korhonen, H., and Malvikko, S.-P.: Characterization of atmospheric trace gas and aerosol concentrations at forest sites in southern and northern Finland using back trajectories, *Boreal Environ. Res.*, 5, 315–336, 2000.
- Kulmala, M., Asmi, A., Lappalainen, H., Carslaw, K., Pöschl, U., Baltensperger, U., Hov, Ø., Brenquier, J.-L., Pandis, S. N., and Facchini, M.: Introduction: European Integrated Project on

- Aerosol Cloud Climate and Air Quality interactions (EUCAARI) – integrating aerosol research from nano to global scales, *Atmos. Chem. Phys.*, 9, 2825–2841, doi:10.5194/acp-9-2825-2009, 2009.
- Kulmala, M., Asmi, A., Lappalainen, H. K., Baltensperger, U., Brenguier, J.-L., Facchini, M. C., Hansson, H.-C., Hov, Ø., O’Dowd, C. D., Pöschl, U., Wiedensohler, A., Boers, R., Boucher, O., de Leeuw, G., Denier van der Gon, H. A. C., Feichter, J., Krejci, R., Laj, P., Lihavainen, H., Lohmann, U., McFiggans, G., Mentel, T., Pilinis, C., Riipinen, I., Schulz, M., Stohl, A., Swietlicki, E., Vignati, E., Alves, C., Amann, M., Ammann, M., Arabas, S., Artaxo, P., Baars, H., Beddows, D. C. S., Bergström, R., Beukes, J. P., Bilde, M., Burkhardt, J. F., Canonaco, F., Clegg, S. L., Coe, H., Crumeyrolle, S., D’Anna, B., Decesari, S., Gilardoni, S., Fischer, M., Fjaeraa, A. M., Fountoukis, C., George, C., Gomes, L., Halloran, P., Hamburger, T., Harrison, R. M., Herrmann, H., Hoffmann, T., Hoose, C., Hu, M., Hyvärinen, A., Hörrak, U., Iinuma, Y., Iversen, T., Josipovic, M., Kanakidou, M., Kiendler-Scharr, A., Kirkevåg, A., Kiss, G., Klimont, Z., Kolmonen, P., Komppula, M., Kristjánsson, J.-E., Laakso, L., Laaksonen, A., Labonnote, L., Lanz, V. A., Lehtinen, K. E. J., Rizzo, L. V., Makkonen, R., Manninen, H. E., McMeeking, G., Merikanto, J., Minikin, A., Mirme, S., Morgan, W. T., Nemitz, E., O’Donnell, D., Panwar, T. S., Pawlowska, H., Petzold, A., Pienaar, J. J., Pio, C., Plass-Duelmer, C., Prévôt, A. S. H., Pryor, S., Reddington, C. L., Roberts, G., Rosenfeld, D., Schwarz, J., Seland, Ø., Sellegri, K., Shen, X. J., Shiraiwa, M., Siebert, H., Sierau, B., Simpson, D., Sun, J. Y., Topping, D., Tunved, P., Vaattovaara, P., Vakkari, V., Veefkind, J. P., Visschedijk, A., Vuollekoski, H., Vuolo, R., Wehner, B., Wildt, J., Woodward, S., Worsnop, D. R., van Zadelhoff, G.-J., Zardini, A. A., Zhang, K., van Zyl, P. G., Kerminen, V.-M., S Carslaw, K., and Pandis, S. N.: General overview: European Integrated project on Aerosol Cloud Climate and Air Quality interactions (EUCAARI) – integrating aerosol research from nano to global scales, *Atmos. Chem. Phys.*, 11, 13061–13143, doi:10.5194/acp-11-13061-2011, 2011.
- Lanz, V., Alfarra, M., Baltensperger, U., Buchmann, B., Hueglin, C., and Prévôt, A.: Source apportionment of submicron organic aerosols at an urban site by factor analytical modelling of aerosol mass spectra, *Atmos. Chem. Phys.*, 7, 1503–1522, doi:10.5194/acp-7-1503-2007, 2007a.
- Lanz, V. A., Alfarra, M. R., Baltensperger, U., Buchmann, B., Hueglin, C., Szidat, S., Wehli, M. N., Wacker, L., Weimer, S., and Caseiro, A.: Source attribution of submicron organic aerosols during wintertime inversions by advanced factor analysis of aerosol mass spectra, *Environ. Sci. Technol.*, 42, 214–220, 2007b.
- Liao, L., Dal Maso, M., Taipale, R., Rinne, J., Ehn, M., Junninen, H., Aijala, M., Nieminen, T., Alekseychik, P., Hulkkonen, M., Worsnop, D. R., Kerminen, V. M., and Kulmala, M.: Monoterpene pollution episodes in a forest environment: indication of anthropogenic origin and association with aerosol particles, *Boreal Environ. Res.*, 16, 288–303, 2011.
- Liu, S., Russell, L., Sueper, D., and Onasch, T.: Organic particle types by single-particle measurements using a time-of-flight aerosol mass spectrometer coupled with a light scattering module, *Atmos. Meas. Tech.*, 6, 187–197, doi:10.5194/amt-6-187-2013, 2013.
- MacQueen, J.: Some methods for classification and analysis of multivariate observations, *Proceedings of the fifth Berkeley symposium on mathematical statistics and probability*, 281–297, 1967.
- Marcolli, C., Canagaratna, M. R., Worsnop, D. R., Bahreini, R., de Gouw, J. A., Warneke, C., Goldan, P. D., Kuster, W. C., Williams, E. J., Lerner, B. M., Roberts, J. M., Meagher, J. F., Fehsenfeld, F. C., Marchewka, M., Bertman, S. B., and Middlebrook, A. M.: Cluster Analysis of the Organic Peaks in Bulk Mass Spectra Obtained During the 2002 New England Air Quality Study with an Aerodyne Aerosol Mass Spectrometer, *Atmos. Chem. Phys.*, 6, 5649–5666, doi:10.5194/acp-6-5649-2006, 2006.
- McQuitty, L. L.: Similarity analysis by reciprocal pairs for discrete and continuous data, *Educ. Psychol. Meas.*, 26, 825–831, 1966.
- Middlebrook, A. M., Bahreini, R., Jimenez, J. L., and Canagaratna, M. R.: Evaluation of composition-dependent collection efficiencies for the aerodyne aerosol mass spectrometer using field data, *Aerosol Sci. Tech.*, 46, 258–271, 2012.
- Mohr, C., Huffman, J. A., Cubison, M. J., Aiken, A. C., Docherty, K. S., Kimmel, J. R., Ulbrich, I. M., Hannigan, M., and Jimenez, J. L.: Characterization of primary organic aerosol emissions from meat cooking, trash burning, and motor vehicles with high-resolution aerosol mass spectrometry and comparison with ambient and chamber observations, *Environ. Sci. Technol.*, 43, 2443–2449, 2009.
- Mohr, C., DeCarlo, P. F., Heringa, M. F., Chirico, R., Slowik, J. G., Richter, R., Reche, C., Alastuey, A., Querol, X., Seco, R., Peñuelas, J., Jiménez, J. L., Crippa, M., Zimmermann, R., Baltensperger, U., and Prévôt, A. S. H.: Identification and quantification of organic aerosol from cooking and other sources in Barcelona using aerosol mass spectrometer data, *Atmos. Chem. Phys.*, 12, 1649–1665, doi:10.5194/acp-12-1649-2012, 2012.
- Murphy, D., Middlebrook, A., and Warshawsky, M.: Cluster analysis of data from the particle analysis by laser mass spectrometry (PALMS) instrument, *Aerosol Sci. Tech.*, 37, 382–391, 2003.
- Murphy, S. M., Sorooshian, A., Kroll, J. H., Ng, N. L., Chhabra, P., Tong, C., Surratt, J. D., Knipping, E., Flagan, R. C., and Seinfeld, J. H.: Secondary aerosol formation from atmospheric reactions of aliphatic amines, *Atmos. Chem. Phys.*, 7, 2313–2337, doi:10.5194/acp-7-2313-2007, 2007.
- Ng, N., Canagaratna, M., Jimenez, J., Zhang, Q., Ulbrich, I., and Worsnop, D.: Real-time methods for estimating organic component mass concentrations from aerosol mass spectrometer data, *Environ. Sci. Technol.*, 45, 910–916, 2010a.
- Ng, N. L., Canagaratna, M. R., Zhang, Q., Jimenez, J. L., Tian, J., Ulbrich, I. M., Kroll, J. H., Docherty, K. S., Chhabra, P. S., Bahreini, R., Murphy, S. M., Seinfeld, J. H., Hildebrandt, L., Donahue, N. M., DeCarlo, P. F., Lanz, V. A., Prévôt, A. S. H., Dinar, E., Rudich, Y., and Worsnop, D. R.: Organic aerosol components observed in Northern Hemispheric datasets from Aerosol Mass Spectrometry, *Atmos. Chem. Phys.*, 10, 4625–4641, doi:10.5194/acp-10-4625-2010, 2010b.
- Ng, N. L., Canagaratna, M. R., Jimenez, J. L., Chhabra, P. S., Seinfeld, J. H., and Worsnop, D. R.: Changes in organic aerosol composition with aging inferred from aerosol mass spectra, *Atmos. Chem. Phys.*, 11, 6465–6474, doi:10.5194/acp-11-6465-2011, 2011.
- Niemi, J. V., Saarikoski, S., Aurela, M., Tervahattu, H., Hillamo, R., Westphal, D. L., Aarnio, P., Koskentalo, T., Makkonen, U., Vehkamäki, H., and Kulmala, M.: Long-range transport episodes

- of fine particles in southern Finland during 1999–2007, *Atmos. Environ.*, 43, 1255–1264, doi:10.1016/j.atmosenv.2008.11.022, 2009.
- Norris, G., Vedantham, R., Wade, K., Brown, S., Prouty, J., and Foley, C.: EPA positive matrix factorization (PMF) 3.0 fundamentals & user guide, Prepared for the US Environmental Protection Agency, Washington, DC, by the National Exposure Research Laboratory, Research Triangle Park, 2008.
- Paatero, P.: Least squares formulation of robust non-negative factor analysis, *Chemometr. Intell. Lab.*, 37, 23–35, 1997.
- Paatero, P.: The multilinear engine – a table-driven, least squares program for solving multilinear problems, including the n-way parallel factor analysis model, *J. Comput. Graph. Stat.*, 8, 854–888, 1999.
- Paatero, P. and Hopke, P. K.: Rotational tools for factor analytic models, *J. Chemometr.*, 23, 91–100, 2009.
- Paatero, P. and Tapper, U.: Analysis of different modes of factor analysis as least squares fit problems, *Chemometr. Intell. Lab.*, 18, 183–194, 1993.
- Paatero, P. and Tapper, U.: Positive matrix factorization: A non-negative factor model with optimal utilization of error estimates of data values, *Environmetrics*, 5, 111–126, 1994.
- Paatero, P., Eberly, S., Brown, S. G., and Norris, G. A.: Methods for estimating uncertainty in factor analytic solutions, *Atmos. Meas. Tech.*, 7, 781–797, doi:10.5194/amt-7-781-2014, 2014.
- Patokoski, J., Ruuskanen, T. M., Hellén, H., Taipale, R., Grönholm, T., Kajos, M. K., Petäjä, T., Hakola, H., Kulmala, M., and Rinne, J.: Winter to spring transition and diurnal variation of vocs in Finland at an urban background site and a rural site, *Boreal Environ. Res.*, 19, 79–103, 2014.
- Patokoski, J., Ruuskanen, T. M., Kajos, M. K., Taipale, R., Rantala, P., Aalto, J., Ryyppö, T., Nieminen, T., Hakola, H., and Rinne, J.: Sources of long-lived atmospheric VOCs at the rural boreal forest site, SMEAR II, *Atmos. Chem. Phys.*, 15, 13413–13432, doi:10.5194/acp-15-13413-2015, 2015.
- Pearson, K.: LIII, On lines and planes of closest fit to systems of points in space, *The London, Edinburgh, and Dublin Philosophical Magazine and Journal of Science*, 2, 559–572, 1901.
- Pierce, S. E., Bell, R. L., Hellberg, R. S., Cheng, C. M., Chen, K. S., Williams-Hill, D. M., Martin, W. B., and Allard, M. W.: Detection and Identification of *Salmonella enterica*, *Escherichia coli*, and *Shigella* spp. via PCR-Electrospray Ionization Mass Spectrometry: Isolate Testing and Analysis of Food Samples, *Appl. Environ. Microb.*, 78, 8403–8411, doi:10.1128/Aem.02272-12, 2012.
- Rebotier, T. P. and Prather, K. A.: Aerosol time-of-flight mass spectrometry data analysis: A benchmark of clustering algorithms, *Anal. Chim. Acta*, 585, 38–54, 2007.
- Reff, A., Eberly, S. I., and Bhave, P. V.: Receptor modeling of ambient particulate matter data using positive matrix factorization: review of existing methods, *J. Air Waste Manage.*, 57, 146–154, 2007.
- Rinne, J., Ruuskanen, T. M., Reissell, A., Taipale, R., Hakola, H., and Kulmala, M.: On-line PTR-MS measurements of atmospheric concentrations of volatile organic compounds in a European boreal forest ecosystem, *Boreal Environ. Res.*, 10, 425–436, 2005.
- Riuttanen, L., Hulkkonen, M., Maso, M. D., Junninen, H., and Kulmala, M.: Trajectory analysis of atmospheric transport of fine particles, SO₂, NO_x and O₃ to the SMEAR II station in Finland in 1996–2008, *Atmos. Chem. Phys.*, 13, 2153–2164, doi:10.5194/acp-13-2153-2013, 2013.
- Rousseeuw, P. J.: Silhouettes: a graphical aid to the interpretation and validation of cluster analysis, *J. Comput. Appl. Math.*, 20, 53–65, 1987.
- Sauer, S. and Kliem, M.: Mass spectrometry tools for the classification and identification of bacteria, *Nat. Rev. Microbiol.*, 8, 74–82, 2010.
- Schade, G. W. and Crutzen, P. J.: Emission of aliphatic amines from animal husbandry and their reactions: Potential source of N₂O and HCN, *J. Atmos. Chem.*, 22, 319–346, 1995.
- Schneider, J., Weimer, S., Drewnick, F., Borrmann, S., Helas, G., Gwaze, P., Schmid, O., Andreae, M., and Kirchner, U.: Mass spectrometric analysis and aerodynamic properties of various types of combustion-related aerosol particles, *Int. J. Mass Spectr.*, 258, 37–49, 2006.
- Shindler, M.: Approximation algorithms for the metric k-median problem, Written Qualifying Exam Paper, University of California, Los Angeles, p. 44, 2008.
- Sintermann, J., Schallhart, S., Kajos, M., Jocher, M., Bracher, A., Münger, A., Johnson, D., Neftel, A., and Ruuskanen, T.: Trimethylamine emissions in animal husbandry, *Biogeosciences*, 11, 5073–5085, doi:10.5194/bg-11-5073-2014, 2014.
- Sogacheva, L., Dal Maso, M., Kerminen, V.-M., and Kulmala, M.: Probability of nucleation events and aerosol particle concentration in different air mass types arriving at Hyytiälä, southern Finland, based on back trajectories analysis, *Boreal Environ. Res.*, 10, 479–491, 2005.
- Sokal, R. R.: A statistical method for evaluating systematic relationships, *Univ. Kans. Sci. Bull.*, 38, 1409–1438, 1958.
- Sokal, R. R. and Sneath, P. H.: Principles of numerical taxonomy, *Principles of numerical taxonomy*, 1963.
- Spath, H.: Cluster analysis algorithms: for data reduction and classification of objects, John Wiley & Sons, 1980.
- Stein, S. E. and Scott, D. R.: Optimization and testing of mass spectral library search algorithms for compound identification, *J. Am. Soc. Mass Spectr.*, 5, 859–866, 1994.
- Steinhaus, H.: Sur la division des corp materiels en parties, *Bull. Acad. Polon. Sci.*, 1, 801–804, 1956.
- Sun, Y.-L., Zhang, Q., Schwab, J. J., Demerjian, K. L., Chen, W.-N., Bae, M.-S., Hung, H.-M., Hogrefe, O., Frank, B., Rattigan, O. V., and Lin, Y.-C.: Characterization of the sources and processes of organic and inorganic aerosols in New York city with a high-resolution time-of-flight aerosol mass spectrometer, *Atmos. Chem. Phys.*, 11, 1581–1602, doi:10.5194/acp-11-1581-2011, 2011.
- Tibshirani, R., Walther, G., and Hastie, T.: Estimating the number of clusters in a data set via the gap statistic, *J. R. Stat. Soc. B*, 63, 411–423, 2001.
- Tukey, J. W.: *Exploratory data analysis*, Addison-Wesley Series in Behavioral Science: Quantitative Methods, Reading, 1977.
- Ulbrich, I. M., Canagaratna, M. R., Zhang, Q., Worsnop, D. R., and Jimenez, J. L.: Interpretation of organic components from Positive Matrix Factorization of aerosol mass spectrometric data, *Atmos. Chem. Phys.*, 9, 2891–2918, doi:10.5194/acp-9-2891-2009, 2009.

- van der Greef, J., Stroobant, P., and van der Heijden, R.: The role of analytical sciences in medical systems biology, *Curr. Opin. Chem. Biol.*, 8, 559–565, 2004.
- Vandeginste, B.: Optimization of analytical information, *TrAC Trends, Anal. Chem.*, 1, 210–215, 1982.
- Weber, R. J., Sullivan, A. P., Peltier, R. E., Russell, A., Yan, B., Zheng, M., De Gouw, J., Warneke, C., Brock, C., and Holloway, J. S.: A study of secondary organic aerosol formation in the anthropogenic-influenced southeastern United States, *J. Geophys. Res.-Atmos.*, 112, D13302, doi:10.1029/2007JD008408, 2007.
- Weimer, S., Alfarra, M., Schreiber, D., Mohr, M., Prévôt, A., and Baltensperger, U.: Organic aerosol mass spectral signatures from wood-burning emissions: Influence of burning conditions and wood type, *J. Geophys. Res.-Atmos.*, 113, D10304, doi:10.1029/2007JD009309, 2008.
- Virkkula, A., Levula, J., Pohja, T., Aalto, P. P., Keronen, P., Schobesberger, S., Clements, C. B., Pirjola, L., Kieloaho, A.-J., Kulmala, L., Aaltonen, H., Patokoski, J., Pumpanen, J., Rinne, J., Ruuskanen, T., Pihlatie, M., Manninen, H. E., Aaltonen, V., Junninen, H., Petäjä, T., Backman, J., Dal Maso, M., Nieminen, T., Olsson, T., Grönholm, T., Aalto, J., Virtanen, T. H., Kajos, M., Kerminen, V.-M., Schultz, D. M., Kukkonen, J., Sofiev, M., De Leeuw, G., Bäck, J., Hari, P., and Kulmala, M.: Prescribed burning of logging slash in the boreal forest of Finland: emissions and effects on meteorological quantities and soil properties, *Atmos. Chem. Phys.*, 14, 4473–4502, doi:10.5194/acp-14-4473-2014, 2014.
- Wishart, D. S.: Current Progress in computational metabolomics, *Brief. Bioinform.*, 8, 279–293, doi:10.1093/bib/bbm030, 2007.
- Zhang, Q., Alfarra, M. R., Worsnop, D. R., Allan, J. D., Coe, H., Canagaratna, M. R., and Jimenez, J. L.: Deconvolution and quantification of hydrocarbon-like and oxygenated organic aerosols based on aerosol mass spectrometry, *Environ. Sci. Technol.*, 39, 4938–4952, 2005.
- Zhang, Q., Jimenez, J. L., Canagaratna, M. R., Ulbrich, I. M., Ng, N. L., Worsnop, D. R., and Sun, Y.: Understanding atmospheric organic aerosols via factor analysis of aerosol mass spectrometry: a review, *Anal. Bioanal. Chem.*, 401, 3045–3067, 2011.